MOLECULAR RECOGNITION OF PET FLUOROIONOPHORES

Kanji Kubo* and Tadamitsu Sakurai†

Institute of Advanced Material Study, 86, Kyushu University, Kasuga-koen, Kasuga, Fukuoka 816-8580, Japan

†*Department of Applied Chemistry, Faculty of Engineering, Kanagawa University, Kanagawa-ku, Yokohama 221-8686, Japan*

Abstract — Recent advances in molecular recognitions of PET fluoroionophores are described.

Contents

Dedicated to Professor Teruaki Muakiyama on the occasion of his 73rd birthday.

1. Introduction

Photoresponsive supramolecular systems are of great significance particularly for their potential application to nanoscale devices for cation sensor and switch.[1] There are extensive investigations toward the characterization of fluoroionophores including crown ether, calixarene, and cyclodextrin derivatives with naphthalene, umbelliferone, anthracene or pyrene fluorophore.[2-5]

Recently, a number of fluoroionophores has been designed for metal ions.[1-5] Most of them operate by a photoinduced electron transfer (PET) mechanism. In a classic example from the de Silva group,[3,4] the binding component of the sensor is *N*-(9-anthrylmethyl)aza-18-crown-6 (**1A**). The uncomplexed fluoroionophore is weakly fluorescent, as the photoexcited fluorophore is quenched by the electron transfer from amino group. Following metal incorporation (Na^+ and K^+), the metal-ligand interaction decreases the amine oxidation potential drastically and prevents the electron transfer. As a consequence, the intense and characteristic anthracene emission is largely restored. However, the Na^+ and K^+ complex of **1A** displayed fluorescence with a low quantum yield. This means the metal induced fluorescence recovery of **1A** is lower than 9-methylanthracene. To design an effective PET fluoroionophore important factors are that the PET fluoroionophores have low emission quantum yield by PET from amine donor to excited chromophore, high emission quantum yield in complexation with guest molecules, selectivity, and stability.

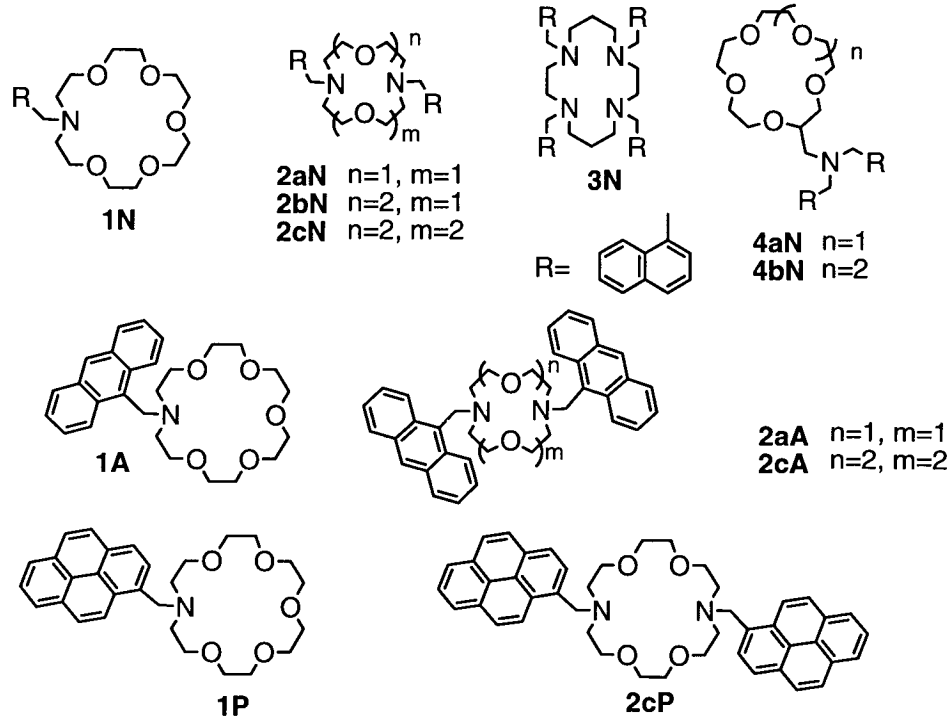

Chart 1.

We are also interested in developing PET fluoroionophore for guest cation using the same supramolecular approach. As an approach to the manipulation of PET fluoroionophore, we now report the fluorescence behavior of the ionophores (**1–4**)[6-12] with some pendants capable of enhancing fluorescence in the presence of guest salts.

2. Design of PET Fluoroionophores

de Silva *et al.* [3,4] have designed an electron donor-spacer-acceptor triad consisting of monoaza-18-crown-6 as a receptor (Figure 1a). Addition of Na^+ and K^+ results in an enhancement of the fluorescence quantum yield of *N*-(9-anthrylmethyl)aza-18-crown-6 by factor of 47. However, the fluorescence quantum yields (ϕ_F=0.053 and 0.14)[3] of **1A**-Na^+ and **1A**-K^+ are lower than that (ϕ_F=0.33)[13] of 9-methylanthracene. In order to design an effective PET fluoroionophore, we propose the ionophores consisting of some donors and acceptors that interact with each other as shown in Figure 1b. The multi-PET system would give weak emission and high CHEF[2] (chelation enhanced fluorescence). Furthermore, as a new approach that takes advantage of the formation of both exciplex and excimer, we reported on the synthesis and fluorescence behavior of diazacrown ether containing two fluorophoric pyrenyl pendants.[6]

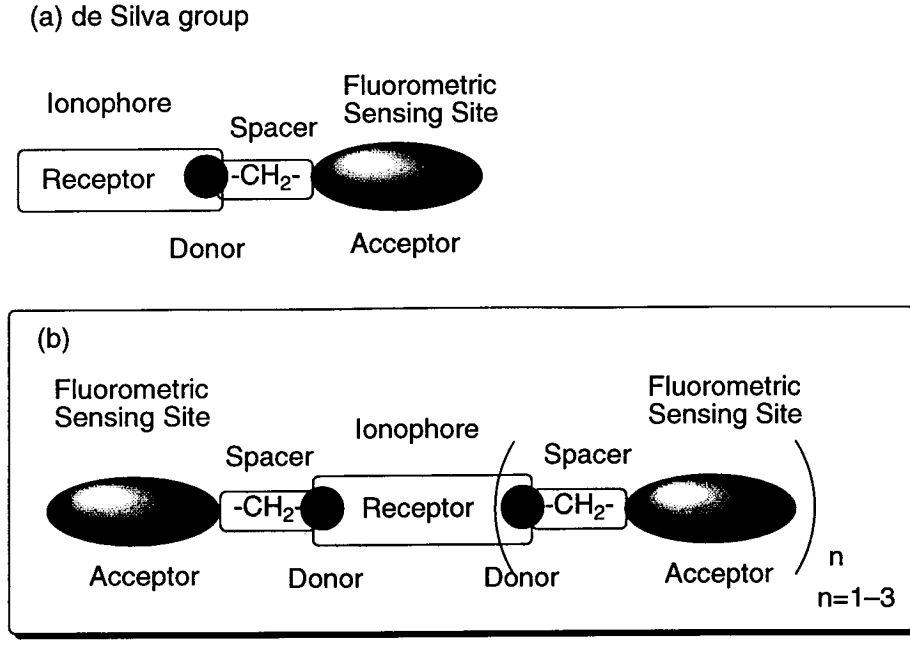

Figure 1. Design of PET fluoroionophores.

3. Fluorescence Properties of PET Fluoroionophores[6-12]

In Figure 2 is illustrated the fluorescence spectral behavior of **1N** (4.0×10^{-5} M, 1 M=1 mol dm^{-3}) and **2cN** (2.0×10^{-5} M) in methanol at room temperature. Fluoroionophores (**1N**) and (**2cN**) (when excited at 280 nm) gave a broad emission band with a maximum at 474 nm in addition to emission band at 335 nm. The formation of an intramolecular exciplex should be responsible for the appearance of the former emission band. The latter emission-band intensities of **1N** and **2cN** were reduced to approximately one-30th and one-440th that of the 1-methylnaphthalene (4.0×10^{-5} M), respectively, accompanied by the occurrence of exciplex fluorescence. This indicates that the quenching of the excited naphthalene chromophore by the azacrown unit proceeds by a mechanism similar to that for the classical naphthalene-aliphatic amine system.[14]

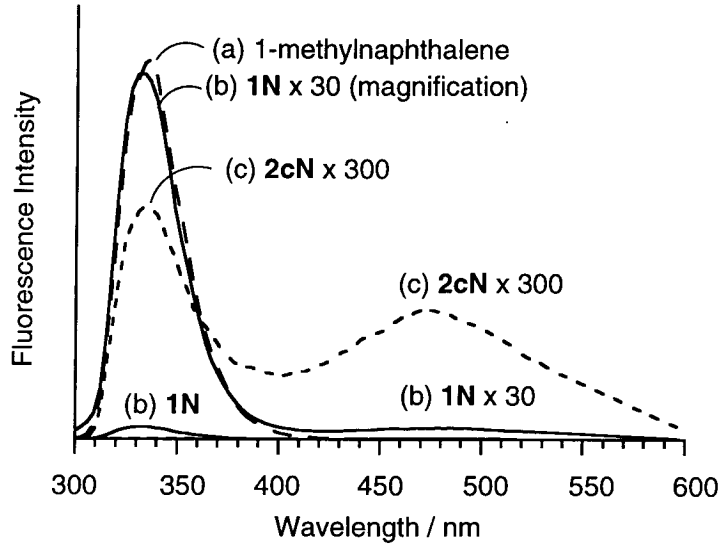

Figure 2. Fluorescence spectra of (a) 1-methylnaphthalene (4.0×10^{-5} M), (b) **1N** (4.0×10^{-5} M), and (c) **2cN** (2.0×10^{-5} M) in methanol at room temperature.

The larger quenching of **2cN** means that the two intramolecular nitrogen atoms and naphthalene rings participate in intramolecular electron transfer in the excited state. The quenching efficiency of excited fluorescent molecule by PET from donor atom is expressed as a relative emission intensity ratio ($I_H/I_{standard}$) of various host molecules and standard substances (1-methylnaphthalene (1-MN) for **1N–4N**, 9-methylanthracene (9-MA) for **1A–2A**, 1-methylpyrene (1-MP) for **1P** and **2cP**) as listed in Table 1.

In diazacrown ether derivatives, the order of the emission intensity ($I_H/I_{standard}$) was **2aN** (1.7×10^{-2}) >

2bN (3.0×10^{-3}) > **2cN** (2.3×10^{-3}). This means that the smaller macrocycle ring inhibits the PET occurring from the nitrogen atoms in the crown to excited fluorescent moieties. The larger $I_{3N}/I_{1\text{-MN}}$ (1.3×10^{-2}) value of cyclam (**3N**) also imply the steric hindrance of four naphthalene rings inhibit the PET. The order of $I_H/I_{standard}$ of the naphthalene derivatives was diaza-18-crown-6 (**2cN**) < diaza-15-crown-5 (**2bN**) < C-armed crown (**4N**) < diaza-12-crown-4 (**2aN**) < cyclam (**3N**) < monoazacrown (**1N**). While, the quenching efficiency ($I_{2aA}/I_{9\text{-MA}}$: 5.1×10^{-3}) of the anthracene-functionalized diaza-12-crown-4 derivative (**2aA**) is similar to that ($I_{2cA}/I_{9\text{-MA}}$: 5.6×10^{-3}) of the corresponding diaza-18-crown-6 (**2cA**). This means the PET from the nitrogen atoms in the crown to excited anthryl rings occur efficiently regardless of the crown ring size.

Table 1. Emission intensity ratio ($I_{1-4}/I_{standard}$) of **1–4** for standard substances*

Compounds		Solvent	Excited / Observed Wavelength (nm)	Exciplex Wavelength (nm)	$I_{1-4}/I_{standard}$	$I_{exciplex}/I_{monomer}$
1N	(4.00×10^{-5} M^{-1})	a	280 / 335	474	3.3×10^{-2}	0.03
2aN	(2.00×10^{-5} M^{-1})	a	280 / 333	474	1.7×10^{-2}	0.08
2bN	(2.00×10^{-5} M^{-1})	a	280 / 335	476	3.0×10^{-3}	0.43
2cN	(2.00×10^{-5} M^{-1})	a	280 / 335	474	2.3×10^{-3}	0.55
3N	(2.00×10^{-5} M^{-1})	b	282 / 337	460	1.3×10^{-2}	0.20
4aN	(2.00×10^{-5} M^{-1})	a	281 / 336	460	3.0×10^{-3}	0.65
4bN	(2.00×10^{-5} M^{-1})	a	281 / 336	458	3.7×10^{-3}	0.30
1A	(1.00×10^{-5} M^{-1})	b	366 / 414	-	2.6×10^{-2}	-
2aA	(5.00×10^{-6} M^{-1})	b	366 / 414	-	5.1×10^{-3}	-
2cA	(5.00×10^{-6} M^{-1})	b	366 / 414	-	5.6×10^{-3}	-
1P	(2.00×10^{-6} M^{-1})	b	340 / 377	464	3.7×10^{-2}	0.40
2cP	(1.00×10^{-6} M^{-1})	b	340 / 377	464	3.7×10^{-3}	1.33

*standard substance: 1-methylnaphthalene (1-MN) for **1N–4N**, 9-methylanthracene (9-MA) for **1A–2A**, 1-methylpyrene (1-MP) for **1P** and **2cP**

a: methanol, b: chloroform : methanol (1:9 *v/v*)

The pyrene derivatives (**1P** and **2cP**) (when excited at 340 nm) gave a broad emission band with a maximum at 464 nm in addition to monomer emission (377 nm) as shown in Figure 3. The formation of an intramolecular exciplex should be responsible for the appearance of the former emission band. The latter emission-band intensities of **1P** and **2cP** were reduced to approximately one-27th and one-270th that of the 1-methylpyrene (2.0×10^{-6} M), respectively, accompanied by the occurrence of exciplex fluorescence, indicating that the quenching of the excited pyrene chromophore by the azacrown unit proceeds by a mechanism similar to that for the classical pyrene-*N,N*-dimethylaniline system[14] or a pyrene-azacrown system.[15]

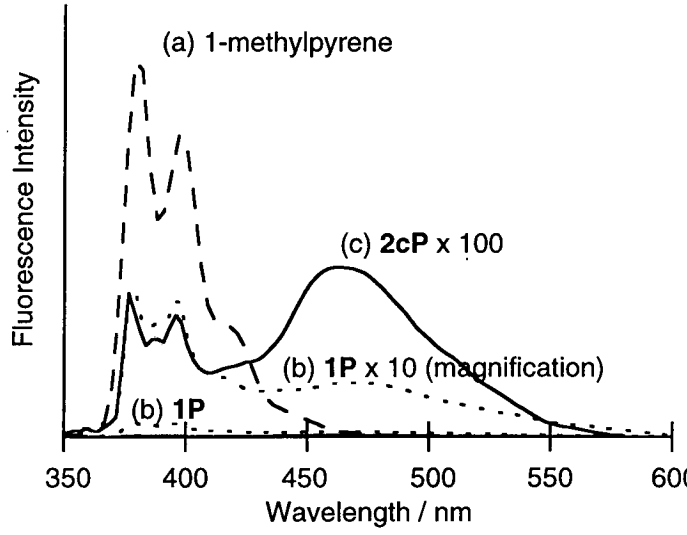

Figure 3. Fluorescence spectra of (a) 1-methylpyrene (2.0×10^{-6} M), (b) **1P** (2.0×10^{-6} M), and (c) **2cP** (1.0×10^{-6} M) in methanol-chloroform (9:1 *v/v*) at room temperature.

4. Complex Formation

4.1. Guest Cation-Induced Fluorescence Enhencement and Recovery

Guest salts enhance the fluorescence quantum yield of **1A** by factors of up to 47.[3] As a measure of the molecular recognition sensing, Czarnik[2] and de Silva *et al.*[3,4] have proposed guest cation-induced fluorescence enhancement factor ($I_{\text{Host-Guest complex}}/I_{\text{Host}}$). However, even if the factor is a big value, if the emission intensity of the complex is far lower than that of standard substance, it isn't fine as PET fluoroionophore. A measure of the guest cation-induced fluorescence recovery ($I_{\text{H-G complex}}/I_{\text{standard}}$) would also be important factor to evaluate PET fluoroionophore. The guest cation-induced fluorescence enhancement and recovery factors ($I_{\text{H-G complex}}/I_{\text{H}}$ and $I_{\text{H-G complex}}/I_{\text{standard}}$) of **1–4** are listed in Table 2. These factors could be utilized as a measure instead of fluorescence quantum yield.

Table 2. Guest cation-induced fluorescence enhancement and recovery factors ($I_{H-G\ complex}/I_H$ and $I_{H-G\ complex}/I_{standard\ substance}$) of **1–4** (**1N–4N**: 2.0 x 10^{-5} M, **1A–2A**: 5.0 x 10^{-6} M, **1P**: 2.0 x 10^{-6} M, **2cP**: 1.0 x 10^{-6} M)

Entry	Guest Salts	Excited / Observed Wavelength (nm)	$I_{H-G\ complex}/I_{standard}$	$I_{H-G\ complex}/I_H$	Log K (M^{-1})
1N	-	280 / 335	3.3 x 10^{-2}	-	- [a]
2.0 x 10^{-5} M	LiSCN	280 / 333	1.0 x 10^{-2}	0.3	3.38 ± 0.06 [a]
	NaSCN	280 / 333	0.3 x 10^{-2}	0.1	3.59 ± 0.03 [a]
	KSCN	280 / 333	1.3 x 10^{-2}	0.4	4.99 ± 0.05 [a]
	RbSCN	280 / 333	1.3 x 10^{-2}	0.4	4.71 ± 0.04 [a]
	CsSCN	280 / 333	1.0 x 10^{-2}	0.3	3.80 ± 0.06 [a]
	NH_4SCN	280 / 333	0.18	5.5	4.20 ± 0.04 [a]
	$Zn(SCN)_2$	280 / 333	0.16	4.9	3.12 ± 0.04 [a]
	$Mg(SCN)_2$	280 / 333	5.9 x 10^{-2}	1.8	4.47 ± 0.02 [a]
	$Ca(SCN)_2$	280 / 333	0.11	3.4	3.85 ± 0.04 [a]
	$Ba(SCN)_2$	280 / 333	0.15	4.5	4.71 ± 0.21 [a]
2aN	-	280 / 333	1.7 x 10^{-2}	-	- [a]
2.0 x 10^{-5} M	LiSCN	280 / 332	1.9 x 10^{-2}	1.1	4.12 ± 0.13 [a]
	NaSCN	280 / 332	2.0 x 10^{-2}	1.2	3.97 ± 0.03 [a]
	KSCN	280 / 332	2.0 x 10^{-2}	1.2	3.97 ± 0.08 [a]
	RbSCN	280 / 332	1.7 x 10^{-2}	1.0	3.71 ± 0.25 [a]
	CsSCN	280 / 332	2.0 x 10^{-2}	1.2	3.69 ± 0.09 [a]
	NH_4SCN	280 / 332	2.9 x 10^{-2}	1.7	3.67 ± 0.02 [a]
	$Zn(SCN)_2$	280 / 332	0.73	43	5.28 ± 0.02 [a]
	$Mg(SCN)_2$	280 / 332	2.7 x 10^{-3}	1.6	4.01 ± 0.02 [a]
	$Ca(SCN)_2$	280 / 332	2.7 x 10^{-2}	1.6	4.33 ± 0.02 [a]
	$Ba(SCN)_2$	280 / 332	2.4 x 10^{-2}	1.4	4.05 ± 0.19 [a]
2bN	-	280 / 335	3.0 x 10^{-3}	-	- [a]
2.0 x 10^{-5} M	LiSCN	280 / 335	3.9 x 10^{-3}	1.3	- [a]
	NaSCN	280 / 335	6.0 x 10^{-3}	2.0	2.39 ± 0.07 [a]

a: methanol, b: methanol:chloroform (9:1 *v/v*)

Table 2. continued

Entry	Guest Salts	Excited / Observed Wavelength (nm)	$I_{H\text{-}G\ complex}/I_{standard}$	$I_{H\text{-}G\ complex}/I_H$	Log K (M^{-1})
2bN	KSCN	280 / 335	4.5×10^{-3}	1.5	- [a]
2.0×10^{-5} M	RbSCN	280 / 335	3.3×10^{-3}	1.1	- [a]
	CsSCN	280 / 335	3.9×10^{-3}	1.3	- [a]
	NH_4SCN	280 / 335	1.4×10^{-2}	4.6	3.34 ± 0.09 [a]
	$Zn(SCN)_2$	280 / 335	2.5×10^{-2}	8.3	2.78 ± 0.05 [a]
	$Mg(SCN)_2$	280 / 335	7.0×10^{-3}	2.3	3.66 ± 0.04 [a]
	$Ca(SCN)_2$	280 / 335	1.5×10^{-2}	4.9	2.90 ± 0.03 [a]
	$Ba(SCN)_2$	280 / 335	1.7×10^{-2}	5.5	2.23 ± 0.23 [a]
2cN	-	280 / 335	2.3×10^{-3}	-	- [a]
2.0×10^{-5} M	LiSCN	280 / 333	3.0×10^{-3}	1.3	1.43 ± 0.09 [a]
	NaSCN	280 / 333	5.0×10^{-3}	2.2	2.09 ± 0.03 [a]
	KSCN	280 / 333	6.4×10^{-3}	2.8	3.27 ± 0.08 [a]
	KSCN	280 / 334	7.6×10^{-3}	3.3	3.45 ± 0.03 [b]
	RbSCN	280 / 333	3.7×10^{-3}	1.6	2.48 ± 0.03 [a]
	CsSCN	280 / 333	2.7×10^{-3}	1.2	1.99 ± 0.16 [a]
	NH_4SCN	280 / 333	1.1×10^{-2}	4.9	3.17 ± 0.05 [a]
	$Zn(SCN)_2$	280 / 333	2.3×10^{-2}	10	2.10 ± 0.05 [a]
	$Mg(SCN)_2$	280 / 333	8.0×10^{-3}	3.5	3.51 ± 0.03 [a]
	$Ca(SCN)_2$	280 / 333	8.5×10^{-2}	37	1.79 ± 0.03 [a]
	$Ba(SCN)_2$	280 / 333	9.3×10^{-2}	41	2.85 ± 0.07 [a]
3N	-	282 / 337	1.3×10^{-2}	-	- [b]
2.0×10^{-5} M	LiSCN	282 / 337	2.3×10^{-2}	1.8	2.87 ± 0.05 [b]
	NaSCN	282 / 337	2.5×10^{-2}	1.9	3.26 ± 0.11 [b]
	KSCN	282 / 337	1.8×10^{-2}	1.4	3.57 ± 0.13 [b]
	RbSCN	282 / 337	3.3×10^{-2}	2.5	3.02 ± 0.08 [b]
	CsSCN	282 / 337	2.2×10^{-2}	1.7	2.89 ± 0.03 [b]
	NH_4SCN	282 / 337	3.4×10^{-2}	2.7	3.11 ± 0.01 [b]

a: methanol, b: methanol:chloroform (9:1 *v/v*)

Table 2. continued

Entry	Guest Salts	Excited / Observed Wavelength (nm)	$I_{H\text{-}G\ complex}/I_{standard}$	$I_{H\text{-}G\ complex}/I_H$	Log K (M^{-1})
3N	$Zn(SCN)_2$	282 / 337	0.11	8.1	3.13 ± 0.03 [b]
2.0×10^{-5} M	$Mg(SCN)_2$	282 / 337	3.3×10^{-2}	2.5	3.50 ± 0.13 [b]
	$Ca(SCN)_2$	282 / 337	2.5×10^{-2}	2.0	3.55 ± 0.06 [b]
	$Ba(SCN)_2$	282 / 337	2.3×10^{-2}	1.8	3.38 ± 0.04 [b]
4aN	-	281 / 334	3.1×10^{-3}	-	- [a]
2.0×10^{-5} M	LiSCN	281 / 334	3.7×10^{-3}	1.2	- [a]
	NaSCN	281 / 334	4.3×10^{-3}	1.4	- [a]
	KSCN	281 / 334	3.7×10^{-3}	1.2	- [a]
	RbSCN	281 / 334	4.3×10^{-3}	1.4	3.49 ± 0.06 [a]
	CsSCN	281 / 334	4.0×10^{-3}	1.3	3.77 ± 0.05 [a]
	NH_4SCN	281 / 334	8.1×10^{-3}	2.6	4.04 ± 0.04 [a]
	$Zn(SCN)_2$	281 / 334	8.4×10^{-3}	2.7	4.57 ± 0.02 [a]
	$Mg(SCN)_2$	281 / 334	6.2×10^{-3}	2.0	4.67 ± 0.05 [a]
	$Ca(SCN)_2$	281 / 334	6.8×10^{-3}	2.2	4.45 ± 0.05 [a]
	$Ba(SCN)_2$	281 / 334	4.7×10^{-3}	1.5	4.46 ± 0.05 [a]
4bN	-	281 / 334	3.7×10^{-3}	-	- [a]
2.0×10^{-5} M	LiSCN	281 / 334	4.4×10^{-3}	1.2	- [a]
	NaSCN	281 / 334	4.4×10^{-3}	1.2	- [a]
	KSCN	281 / 334	4.8×10^{-3}	1.3	- [a]
	RbSCN	281 / 334	4.8×10^{-3}	1.3	3.93 ± 0.04 [a]
	CsSCN	281 / 334	5.2×10^{-3}	1.4	3.00 ± 0.39 [a]
	NH_4SCN	281 / 334	5.2×10^{-3}	1.4	4.28 ± 0.18 [a]
	$Zn(SCN)_2$	281 / 334	8.9×10^{-3}	2.4	3.56 ± 0.05 [a]
	$Mg(SCN)_2$	281 / 334	5.9×10^{-3}	1.6	3.81 ± 0.05 [a]
	$Ca(SCN)_2$	281 / 334	5.9×10^{-3}	1.6	4.00 ± 0.12 [a]
	$Ba(SCN)_2$	281 / 334	4.4×10^{-3}	1.2	- [a]
1A	-	366 / 414	2.6×10^{-2}	-	- [a]

a: methanol, b: methanol:chloroform (9:1 *v/v*)

Table 2. continued

Entry	Guest Salts	Excited / Observed Wavelength (nm)	$I_{H\text{-}G\ complex}/I_{standard}$	$I_{H\text{-}G\ complex}/I_{H}$	Log K (M^{-1})
1A	LiSCN	368 / 419	0.14	5.2	3.30 ± 0.01 [a]
5.0×10^{-6} M	NaSCN	368 / 418	5.5×10^{-2}	2.1	3.77 ± 0.15 [a]
	KSCN	368 / 415	0.22	8.4	5.07 ± 0.09 [a]
	RbSCN	368 / 415	0.19	7.2	4.21 ± 0.06 [a]
	CsSCN	368 / 417	0.10	4.0	3.98 ± 0.06 [a]
	NH_4SCN	368 / 417	0.31	12	3.99 ± 0.04 [a]
	$Zn(SCN)_2$	368 / 422	0.31	12	2.67 ± 0.04 [a]
	$Mg(SCN)_2$	368 / 421	0.20	7.8	3.63 ± 0.05 [a]
	$Ca(SCN)_2$	368 / 422	0.23	8.7	3.57 ± 0.10 [a]
	$Ba(SCN)_2$	368 / 419	0.31	12	3.56 ± 0.01 [a]
2aA	-	366 / 414	5.1×10^{-3}	-	- [b]
5.0×10^{-6} M	LiSCN	366 / 415	6.1×10^{-3}	1.2	- [b]
	NaSCN	366 / 414	6.6×10^{-3}	1.3	- [b]
	KSCN	366 / 413	6.6×10^{-3}	1.3	- [b]
	RbSCN	366 / 416	5.1×10^{-3}	1.0	- [b]
	CsSCN	366 / 415	5.5×10^{-3}	1.1	- [b]
	NH_4SCN	366 / 417	1.7×10^{-2}	3.3	3.26 ± 0.05 [b]
	$Zn(SCN)_2$	366 / 416	0.93	182	4.46 ± 0.09 [b]
	$Mg(SCN)_2$	366 / 416	1.9×10^{-2}	3.7	3.13 ± 0.09 [b]
	$Ca(SCN)_2$	366 / 417	2.1×10^{-2}	4.2	3.58 ± 0.04 [b]
	$Ba(SCN)_2$	366 / 417	1.1×10^{-2}	2.2	3.24 ± 0.05 [b]
2cA	-	366 / 414	5.6×10^{-3}	-	- [b]
5.0×10^{-6} M	LiSCN	366 / 414	7.8×10^{-3}	1.4	0.78 ± 0.08 [b]
	NaSCN	366 / 413	4.8×10^{-2}	8.6	2.70 ± 0.10 [b]
	KSCN	366 / 414	0.15	27	3.29 ± 0.17 [b]
	RbSCN	366 / 414	6.2×10^{-2}	11	2.65 ± 0.05 [b]
	CsSCN	366 / 415	1.6×10^{-2}	2.8	2.11 ± 0.03 [b]

a: methanol, b: methanol:chloroform (9:1 *v/v*)

Table 2. continued

Entry	Guest Salts	Excited / Observed Wavelength (nm)	$I_{H\text{-}G\ complex}/I_{standard}$	$I_{H\text{-}G\ complex}/I_{H}$	Log K (M^{-1})
2cA	NH_4SCN	366 / 420	4.1×10^{-2}	7.4	2.08 ± 0.04 [b]
5.0×10^{-6} M	$Zn(SCN)_2$	366 / 421	7.3×10^{-2}	13	0.85 ± 0.15 [b]
	$Mg(SCN)_2$	366 / 417	1.8×10^{-2}	3.2	3.07 ± 0.08 [b]
	$Ca(SCN)_2$	366 / 415	4.9×10^{-2}	8.7	0.48 ± 0.18 [b]
	$Ba(SCN)_2$	366 / 417	2.8×10^{-2}	5.0	1.77 ± 0.06 [b]
1P	-	340 / 377	3.7×10^{-2}	-	- [b]
2.0×10^{-6} M	LiSCN	340 / 396	0.17	4.5	1.68 ± 0.03 [b]
	NaSCN	340 / 378	2.2×10^{-2}	0.6	3.00 ± 0.02 [b]
	KSCN	340 / 392	0.20	5.3	4.75 ± 0.02 [b]
	RbSCN	340 / 395	0.14	3.9	4.17 ± 0.01 [b]
	CsSCN	340 / 396	9.6×10^{-2}	2.6	3.67 ± 0.03 [b]
	NH_4SCN	340 / 395	0.29	7.7	3.40 ± 0.01 [b]
	$Zn(SCN)_2$	340 / 377	0.56	15	2.20 ± 0.04 [b]
	$Mg(SCN)_2$	340 / 378	0.34	9.2	2.71 ± 0.02 [b]
	$Ca(SCN)_2$	340 / 395	0.31	8.5	2.93 ± 0.04 [b]
	$Ba(SCN)_2$	340 / 396	0.31	8.5	4.35 ± 0.01 [b]
2cP	-	340 / 377	3.7×10^{-3}	-	- [b]
1.0×10^{-6} M	LiSCN	340 / 378	2.7×10^{-2}	7.3	0.48 ± 0.07 [b]
		340 / 459	-	1.4	- [b]
	NaSCN	340 / 395	2.7×10^{-2}	7.3	2.59 ± 0.04 [b]
		340 / 462	-	14	- [b]
	KSCN	340 / 396	0.10	27	3.38 ± 0.01 [b]
		340 / 447	-	14	- [b]
	RbSCN	340 / 395	3.6×10^{-2}	9.6	2.54 ± 0.03 [b]
		340 / 444	-	5.8	- [b]
	CsSCN	340 / 396	2.1×10^{-2}	5.8	2.07 ± 0.01 [b]
		340 / 446	-	1.6	- [b]

a: methanol, b: methanol:chloroform (9:1 *v/v*)

Table 2. continued

Entry	Guest Salts	Excited / Observed Wavelength (nm)	$I_{H\text{-}G\ complex}/I_{standard}$	$I_{H\text{-}G\ complex}/I_H$	Log K (M^{-1})
2cP	NH_4SCN	340 / 378	7.0×10^{-2}	19	1.70 ± 0.04 [b]
1.0×10^{-6} M		340 / 474	-	3.2	- [b]
	$Zn(SCN)_2$	340 / 378	0.11	29	0.85 ± 0.07 [b]
		340 / 466	-	4.5	- [b]
	$Mg(SCN)_2$	340 / 378	1.6×10^{-2}	4.4	3.15 ± 0.05 [b]
		340 / 446	-	1.4	- [b]
	$Ca(SCN)_2$	340 / 395	5.5×10^{-2}	15	2.16 ± 0.04 [b]
		340 / 446	-	2.0	- [b]
	$Ba(SCN)_2$	340 / 396	0.14	37	2.15 ± 0.05 [b]
		340 / 446	-	3.8	- [b]

standard: standard substance (1-methylnaphthalene (1-MN) for **1N–4N**, 9-methylanthracene (9-MA) for **1A–2A**, 1-methylpyrene (1-MP) for **1P** and **2cP**)

a: methanol, b: methanol:chloroform (9:1 *v/v*)

4.2. Monoaza-18-crown-6 Ether (1N)[12]

In Figure 4 is illustrated the fluorescence spectral behavior of **1N** (2.0×10^{-5} M) in methanol at room temperature. A dramatic change in the emission intensity of **1N** (I_{1N}) was observed upon the addition of various kinds of guest cations (Li^+, Na^+, K^+, Rb^+, Cs^+, NH_4^+, Zn^{2+}, Mg^{2+}, Ca^{2+}, and Ba^{2+}).

When the guest salts were added, the relative emission intensity ratio ($I_{H\text{-}G\ complex}$ /I_{1N}) changed from 0.1 to 5.5 depending on the nature of guest cations. Clearly, the emission intensity changes with an increase in the guest cation concentration. The intensity ratio ($I_{H\text{-}G\ complex}$ /I_{1N}) was different among bound guest cations and was decreased in the following order: NH_4^+ (5.5) > Zn^{2+} (4.9) > Ba^{2+} (4.5) > Ca^{2+} (3.4) > Mg^{2+} (1.8) > Rb^+ (0.42) > K^+ (0.38) > Cs^+ (0.31) > Li^+ (0.28) > Na^+ (0.09). It is clearly seen from Figure 4 that the emission intensity increased in the presence of the bivalent metal ions and ammonium ion, except for alkali metal ions. The observed enhancement indicates the inhibition of exciplex formation by complexation with a guest salt. Furthermore, it is noteworthy that the **1N**-alkali thiocyanate complex exhibited a decrease in its emission intensity relative to that of **1N**, itself. This suggests that the observed quenching is due to the presence of thiocyanate ion. A similar quenching by

the thiocyanate anion was explained based on the photoinduced electron transfer from this anion to the naphthalene chromophore.[1,16]

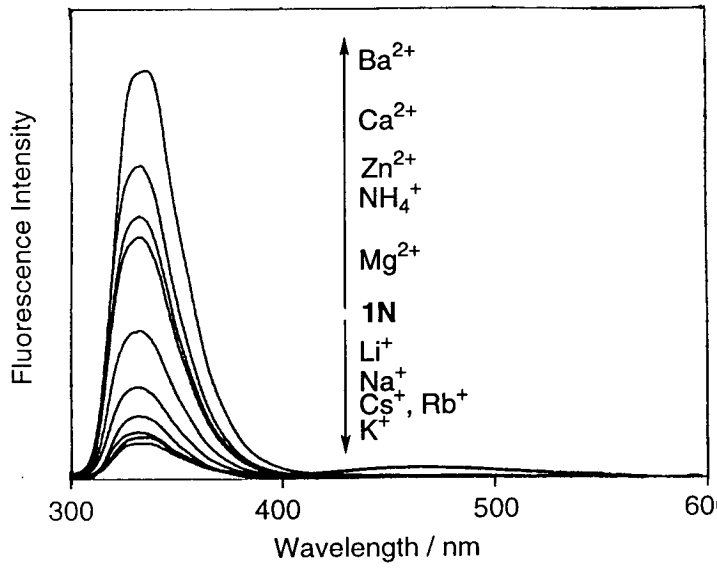

Figure 4. Fluorescence spectra of **1N** (2.00 x 10^{-5} M) with and without guest salts (4.00 x 10^{-4} M) in methanol.

4.3. Diazacrown Ethers (2N)[7] and Azamacrocycle (3N)[9]

Fluorescence Spectroscopy

The diaza-18-crown-6 derivative (**2cN**) displayed a remarkable emission enhancement in the presence of guest salts as shown in Figure 5.

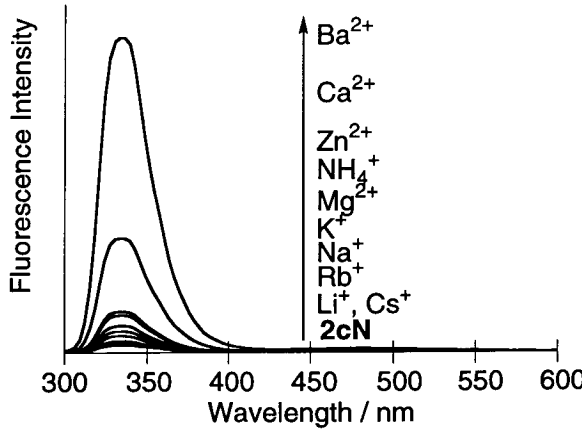

Figure 5. Fluorescence spectra of **2cN** (2.00 x 10^{-5} M) with and without various metal salts (1.00 x 10^{-2} M) in methanol, as excited at 280 nm.

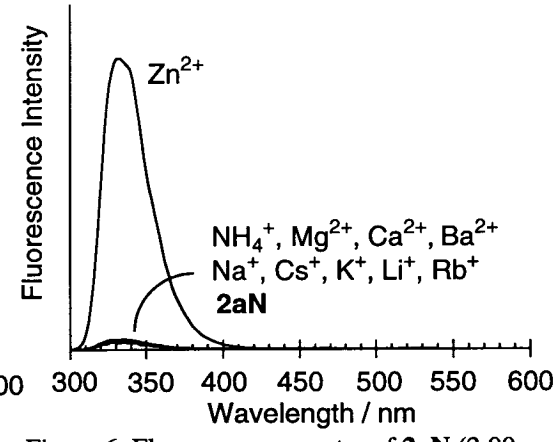

Figure 6. Fluorescence spectra of **2aN** (2.00 x 10^{-5} M) with and without various guest salts (5.00 x 10^{-4} M) in methanol, as excited at 280 nm.

The relative emission intensity enhancement ($I_{\text{H-G complex}}/I_{\text{2cN}}$) changed from 1.1 to 41 depending on the

nature of guest salts. The intensity ratio ($I_{\text{H-G complex}}/I_{\mathbf{2cN}}$) was different among bound guest cations and was decreased in the following order: Ba^{2+} (41) > Ca^{2+} (37) > Zn^{2+} (10) > NH_4^+ (4.9) > Mg^{2+} (3.5) > K^+ (2.8) > Na^+ (2.2) > Rb^+ (1.6) > Li^+ (1.3) > Cs^+ (1.2). The larger $I_{\text{H-G complex}}/I_{\mathbf{2cN}}$ value for bivalent metal ions than for monovalent ions suggests that the coordinated structure of bivalent metal ions differs from that of the alkali metal ions. The nitrogen atom is very likely to prefer coordination with bivalent metal ions.

It is clearly seen from Figure 6 that the diaza-12-crown-4 derivative (**2aN**) exhibited Zn^{2+} fluorescence enhancement selectivity. The $I_{\text{H-G complex}}/I_{\mathbf{2aN}}$ value was different among bound guest cations and decreased in the following order: Zn^{2+} (43) > NH_4^+ (1.7) > Mg^{2+}, Ca^{2+} (1.6) > Ba^{2+} (1.4) > Na^+, K^+, Cs^+ (1.2) > Li^+ (1.1) > Rb^+ (1.0). Zinc ion binding could then cause recovery. This high fluorescence recovery is due to strong coordination from the nitrogen atoms of the diazacrown to the zinc ion. The fluorescence recovery ($I_{\text{H-G complex}}/I_{\text{1-MN}}$) of **2aN**-$Zn(SCN)_2$ was larger than that of **2cN**-$Ba(SCN)_2$ (Figure 7). The highest guest cation-induced emission intensity can be used as a measure of switch-on ability of PET fluoroionopohre. The order of guest cation-induced emission intensity enhancemet ($I_{\text{H-G complex}}/I_{\text{H}}$) and recovery ($I_{\text{H-G complex}}/I_{\text{1-MN}}$) with respect to the specific cation for each fluoroionophore were **2aN** > **2cN** > **2bN** > **3N** > **1N** > **4aN** > **4bN** and **2aN** > **1N** > **3N** > **2cN** > **2bN** > **4bN** > **4aN**. This result suggests that the diaza-12-crown-4 derivative (**2aN**) is the most excellent PET fluoroionophore in the naphthalene-functionalized azamacrocycles (**1N**–**4N**).

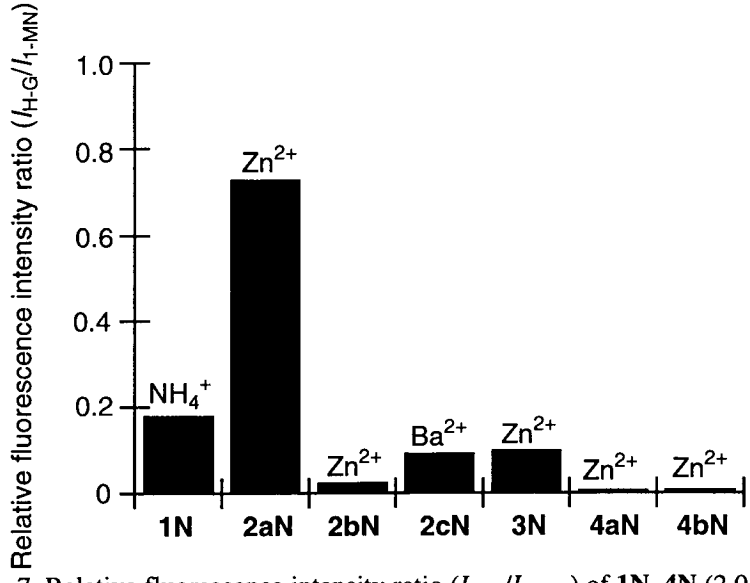

Figure 7. Relative fluorescence intensity ratio ($I_{\text{H-G}}/I_{\text{1-MN}}$) of **1N**–**4N** ($2.0 \times 10^{-5}$ M) with respect to the specific cation for each fluoroionopohre; $[NH_4^+] = 2.0 \times 10^{-4}$ M for **1N**, $[Ba^{2+}] = 2.0 \times 10^{-2}$ M for **2cN**, $[Zn^{2+}] = 2.0 \times 10^{-4}$ M for **2aN**, 1.0×10^{-2} M for **2bN**, 5.0×10^{-3} M for **3N**, 1.0×10^{-3} M for **4aN**, and 1.0×10^{-3} M for **4bN**

NMR Spectral Analysis

Binding interactions of the host (**2cN**) with alkali metal and bivalent metal ions were examined using ^{1}H NMR spectroscopy. When alkali metal ions were added, each resonance peak was shifted to downfield or upfield depending on the nature of added metal ions (Figure 8), while the addition of bivalent metal ions decreased the original-signal intensities with an increase in new-signal intensities (Figure 8).

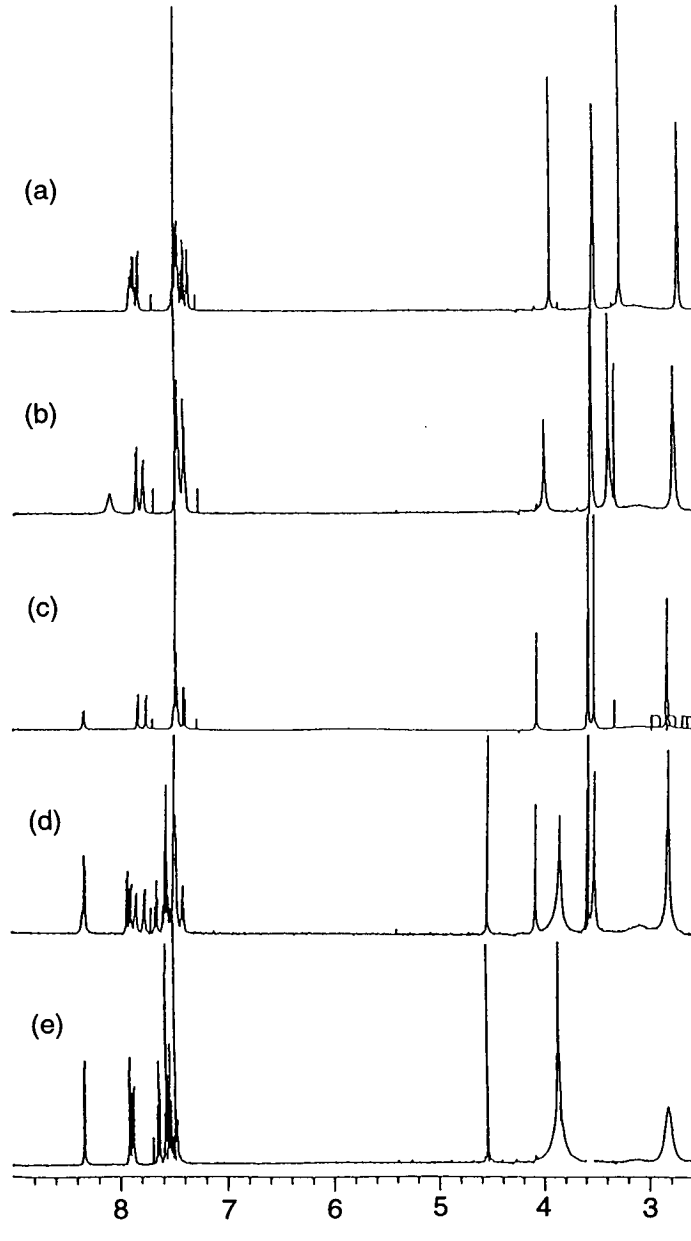

Figure 8. ^{1}H NMR spectral changes of **2cN** (8.0 x 10^{-4} M) with (a) KSCN (5.6 x 10^{-4} M), (b) KSCN (1.4 x 10^{-3} M), (c) 0, (d) $Ba(SCN)_2$ (1.4 x 10^{-3} M), and (e) $Ba(SCN)_2$ (5.6 x 10^{-4} M) in CD_3CN-$CDCl_3$ (1:1 *v/v*) at 298 K.

These spectral changes confirm that the exchange rates are different between alkali metal and bivalent metal ions. The gradual upfield shift of proton signals in the azacrown unit with added KSCN (Figure 8) shows that the exchange process between free host and its potassiun complex is rapid as compared to the NMR time scale: Time-averaged NMR shifts are observed depending upon the guest concentrations. On the other hand, the original (free host, **2cN**) signal intensities decreased and the intensities of new signals (of the corresponding complex **2cN**-Ba^{2+}) at 3.86 and 4.55 ppm increased as the $Ba(SCN)_2$ concentration was increased (Figure 8). Thus, the exchange process for this complex is slow enough even at room temperature, compared with the NMR time scale, to give new signals corresponding to the barium complex (**2cN**-Ba^{2+}). The difference in exchange rate between K^+ and Ba^{2+} should be responsible for a large difference in the relative emission-intensity ratio for these guest cations (Figure 5).

In all of the complexation systems, the examined composition of the complexes [**2cN**- guest salt] could fortunately be determined by using the ^1H NMR titration curve. Figure 9 shows a plot of the induced shift of each signal versus the molar composition of **2cN** and the guest. The stoichiometry of the complexation between the host **2cN** and the guest K^+ was confirmed to be 1:1, at least, in a chloroform-*d* and acetonitrile-d_3 (1:1 *v/v*) mixture. Similarly, the composition of the **2cN**-metal cation complexes (Li^+, Na^+, K^+, Rb^+, Cs^+, Mg^{2+}, Ca^{2+} and Ba^{2+}) was determined as 1:1 by the molar ratio.

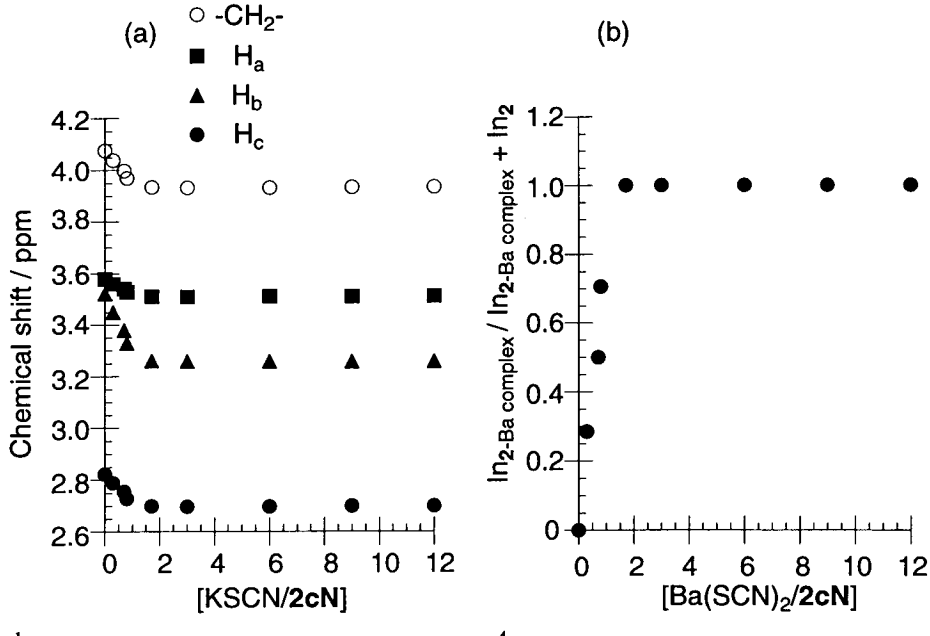

Figure 9. ^1H NMR spectral changes of **2cN** (8.0×10^{-4} M) with KSCN and $Ba(SCN)_2$ in $CDCl_3$-CD_3CN (1:1 *v/v*); In_{2cN}: Integral ratio of free (**2cN**), $In_{2cN\text{-}Ba\ complex}$: Integral ratio of **2cN**-$Ba(SCN)_2$ complex.

Table 3. Changes of ^{1}H NMR chemical shifts of **2cN** (1.0×10^{-2} M) with various guest salts (1.0×10^{-2} M) in $CDCl_3$-CD_3CN (1:1 *v/v*)

	Naphthylmethyl unit		Azacrown unit		
	H-8	-CH_2-	H_a	H_b	H_c
2cN	8.35	4.08	3.58	3.52	2.82
LiSCN	8.24 (-0.11)	4.12 (+0.04)	3.61 (+0.03)	3.55 (+0.03)	2.81 (-0.01)
NaSCN	7.95 (-0.40)	3.89 (-0.19)	3.49 (-0.09)	3.16 (-0.36)	2.66 (-0.16)
KSCN	7.93 (-0.42)	3.94 (-0.14)	3.51 (-0.07)	3.26 (-0.26)	2.70 (-0.12)
RbSCN	8.08 (-0.27)	3.98 (-0.10)	3.53 (-0.05)	3.34 (-0.18)	2.73 (-0.09)
CsSCN	8.24 (-0.11)	4.03 (-0.05)	3.56 (-0.02)	3.46 (-0.06)	2.78 (-0.04)
NH_4SCN	8.14 (-0.21)	4.05 (-0.03)	3.56 (-0.02)	3.32 (-0.20)	2.79 (-0.03)
$Zn(SCN)_2$	8.29 (-0.06)	4.27 (+0.19)	3.60 (+0.02)	3.43 (-0.09)	2.97 (+0.15)
$Mg(SCN)_2$	8.24 (-0.11)	4.39 (+0.31)	3.63 (+0.05)	3.41 (-0.11)	3.06 (+0.24)
$Ca(SCN)_2$	8.55 (+0.20)	4.87 (+0.79)	3.84 (+0.26)	3.84 (+0.32)	2.85 (+0.03)
$Ba(SCN)_2$	8.35 (0.00)	4.55 (+0.47)	3.86 (+0.28)	3.86 (+0.34)	2.82 (0.00)

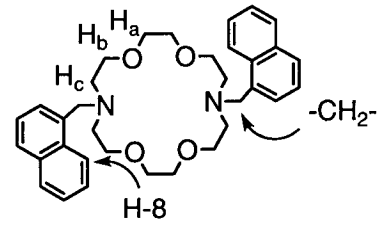

The chemical (δ) and induced ($\Delta\delta$) shifts of the host (**2cN**) with and without guest salts are summarized in Table 3. The presence of Ba^{2+} and Ca^{2+} induced a dramatic downfield shift ($\Delta\delta$= 0.47 for Ba^{2+} and 0.79 for Ca^{2+}) of the methylene proton signal of 1-naphthylmethyl group. There was also a significant downfield shift ($\Delta\delta$= 0.34 for Ba^{2+} and 0.32 for Ca^{2+}) of the H_b signal of azacrown unit. These downfield shifts may be due to the strong interaction of the cations with the azacrown nitrogen. On the other hand, Na^+, K^+, Rb^+ and Cs^+ caused distinct upfield shifts of the H_b signal of azacrown unit as well as the methylene proton signal of 1-naphthylmethyl group. Ring-current effects of the naphthalene rings must be responsible for these upfield shifts.

Further detailed information on the cation binding behavior for **2cN** was obtained by ^{13}C NMR spectroscopy in chloroform-*d* and acetonitrile-d_3 (1:1 *v/v*) mixture. Table 4 summarizes the cation-induced shifts of the selected carbon signals of **2cN**. In order to assign the carbon signals of **2cN** in the absence and presence of the guest salt, H-H and C-H COSY experiments were performed for the free host as well as for each of the complexes (Figure 10).

Table 4. Changes of ^{13}C NMR chemical shifts of **2cN** (1.0×10^{-2} M) with various guest salts (1.0×10^{-2} M) in $CDCl_3$-CD_3CN (1:1 *v/v*)

		Azacrown unit		
	$-CH_2-$	C_a	C_b	C_c
2cN	58.8	71.0	70.2	54.6
LiSCN	57.5 (-1.3)	69.5 (-1.5)	69.4 (-0.8)	53.5 (-1.1)
NaSCN	56.9 (-1.9)	68.6 (-2.4)	67.7 (-2.5)	53.3 (-1.3)
KSCN	56.9 (-1.9)	69.8 (-1.2)	68.0 (-2.2)	55.7 (+1.1)
RbSCN	57.1 (-1.7)	70.1 (-0.9)	68.5 (-1.7)	55.5 (+0.9)
CsSCN	58.1 (-0.7)	70.6 (-0.4)	69.5 (-0.7)	55.0 (+0.4)
NH_4SCN	55.2 (-3.6)	68.9 (-2.1)	66.9 (-3.3)	55.1 (+0.5)
$Zn(SCN)_2$	57.3 (-1.5)	70.5 (-0.5)	67.7 (-2.5)	55.3 (+0.7)
$Mg(SCN)_2$	55.2 (-3.6)	68.9 (-2.1)	65.9 (-4.3)	54.1 (-0.5)
$Ca(SCN)_2$	53.4 (-5.4)	70.3 (-0.7)	69.6 (-0.6)	51.0 (-3.6)
$Ba(SCN)_2$	49.7 (-9.1)	70.9 (-0.1)	68.4 (-1.8)	53.3 (-1.3)

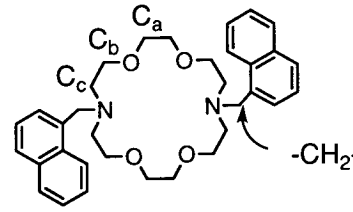

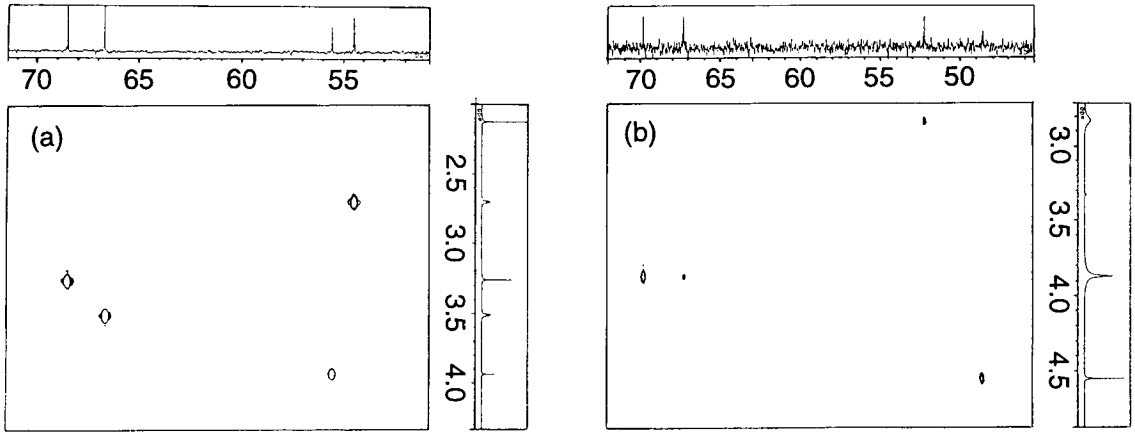

Figure 10. C-H COSY specta of **2cN** (1.0×10^{-2} M) with (a) KSCN (1.0×10^{-2} M) and (b) $Ba(SCN)_2$ (1.0×10^{-2} M) in $CDCl_3$-CD_3CN (1:1 *v/v*).

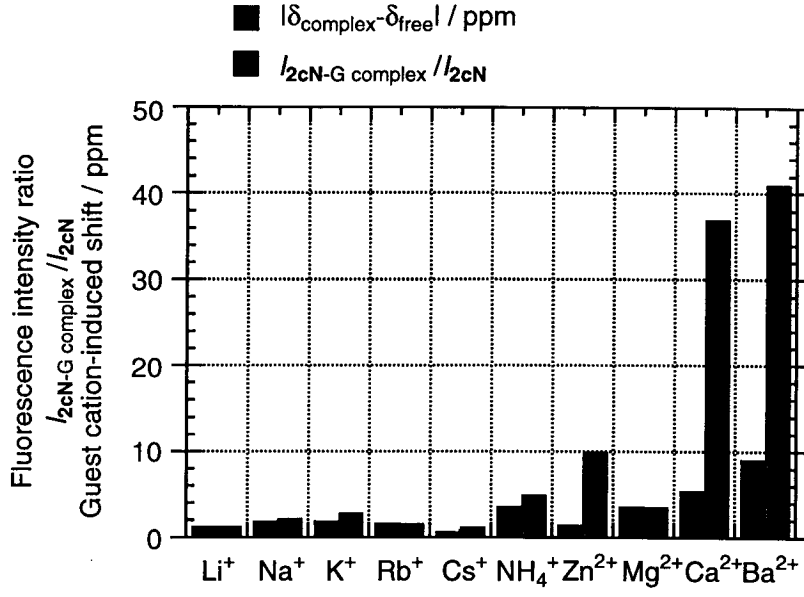

Figure 11. Guest cation-induced changes in ^{13}C NMR chemical shift of methylene carbon of naphthylmethyl group ([**2cN**] =1.0 x 10^{-2} M) and in emission intensity ratio ($I_{2cN\text{-}G\ complex}/I_{2cN}$, [**2cN**] = 2.0 x 10^{-5} M); [Guest cations] = 1.0 x 10^{-2} M.

Interestingly, Ba^{2+} produced even more remarkable chemical-shift change for the methylene carbon signal (Figure 11). The magnitude of guest cation-induced shift for this carbon signal decreased in the following order: Ba^{2+} (-9.1) > Ca^{2+} (-5.4) > NH_4^+, Mg^{2+} (-3.6) > Na^+, K^+ (-1.9) > Rb^+ (-1.7) > Zn^{2+} (-1.5) > Li^+ (-1.3), Cs^+ (-0.7), clearly demonstrating that the nitrogen atom in the azacrown ether has a propensity to strongly coordinate with bivalent metal ions.

4.4. C-Armed Crown Ethers (4N)[11]

C-Armed crown ethers (**4N**) also exhibited Zn^{2+} fluorescence enhancement selectivity (Table 2). However, the changes were too small. The orders of intensity ratio ($I_{H\text{-}G\ complex}/I_{4N}$) were **4aN**: Zn^{2+} (2.7) > NH_4^+ (2.6) > Ca^{2+} (2.2) > Mg^{2+} (2.0) > Ba^{2+} (1.5) > Na^+, Rb^+ (1.4) > Cs^+ (1.3) > Li^+, K^+ (1.2), **4bN**: Zn^{2+} (2.4) > Ca^{2+}, Mg^{2+} (1.6) > NH_4^+, Cs^+ (1.4) > Rb^+, K^+ (1.3) > Ba^{2+},

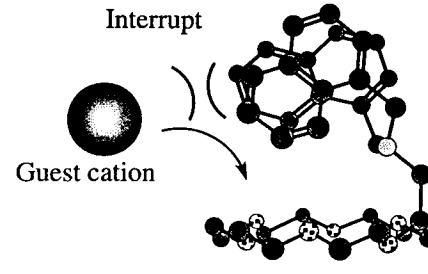

Figure 12. Structure of **4bN** generated by MM2 calculation.

Na^+, Li^+ (1.2)).

The fluorescence recoveries ($I_{\mathbf{4aN}\text{-Zn complex}}/I_{\text{1-MN}}$=8.9 x 10^{-3}, $I_{\mathbf{4bN}\text{-Zn complex}}/I_{\text{1-MN}}$=8.4 x 10^{-3}) of the C-armed crowns (**4N**) for Zn^{2+} were lower than that of the *N,N',N'',N'''*-tetrakis(1-naphthylmethyl)-cyclam ($I_{\mathbf{3N}\text{-Zn complex}}/I_{\text{1-MN}}$=0.11)[9] and *N,N'*-bis(1-naphthylmethyl)diaza-12-crown-4 ($I_{\mathbf{2aN}\text{-Zn complex}}/I_{\text{1-MN}}$=0.73).[10] The association constants of **4bN** for guest cations were also lower than those[17] of 18-crown-6. This means that the two naphthyl groups inhibit the complexation between guest cation and nitrogen atom of side arm as shown in Figure 12.

4.5. Anthracene Derivatives (1A, 2A)[8]

N,N'-Bis(9-anthrylmethyl)diaza-18-crown-6 (**2cA**) exhibited K^+ fluorescence enhancement selectivity (Figure 13). The order of $I_{\text{H-G complex}}/I_{\mathbf{2cA}}$ (K^+ (27) > Zn^{2+} (13) > Rb^+ (11) > Ca^{2+} (8.7) > Na^+ (8.6) > NH_4^+ (7.4) > Ba^{2+} (5.0) > Mg^{2+} (3.2) > Cs^+ (2.8) > Li^+ (1.4)) differs from that of $I_{\text{H-G complex}}/I_{\mathbf{1A}}$ (Zn^{2+}, Ba^{2+}, K^+ (12) > Ca^{2+} (8.7) > K^+ (8.4) > Mg^{2+} (7.8) > Rb^+ (7.2) > Li^+ (5.2) > Cs^+ (4.0) > Na^+ (2.1)). However, the fluorescence recoveries ($I_{\text{H-G complex}}/I_{\text{9-MA}}$) and association constants of the diaza-18-crown-6 derivative (**2cA**) were lower than those of **1A**, suggesting that the two anthracene rings inhibit the complexation between guest salts and azacrown ether.

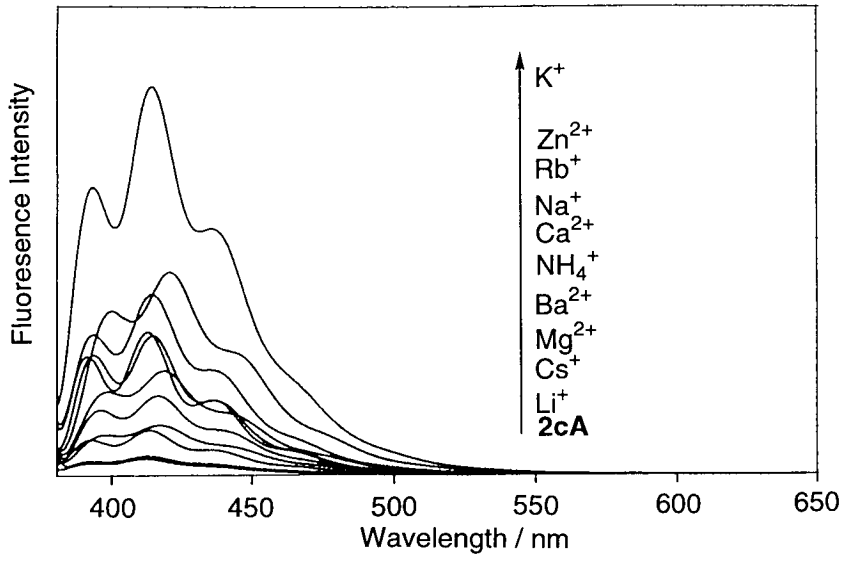

Figure 13. Fluorescence spectra of **2cA** (5.00 x 10^{-6} M) with and without guest salts (5.00 x 10^{-2} M) in methanol-chloroform (9:1 *v/v*).

A dramatic change in the emission intensity of the diaza-12-crown-4 derivative (**2aA**) was observed upon the addition of Zn^{2+} as shown in Figure 14. In the presence of this cation the host fluorescence intensity was increased by a factor of 182. The emission intensity ratio ($I_{\text{H-G complex}}/I_{\mathbf{2aA}}$) was different among

bound guest cations and decreased in the following order: Zn^{2+} (182) > Ca^{2+} (4.2) > Mg^{2+} (3.7) > NH_4^+ (3.3) > Ba^{2+} (2.2) > Na^+, K^+ (1.3) > Li^+ (1.2) > Cs^+ (1.1) > Rb^+ (1.0).

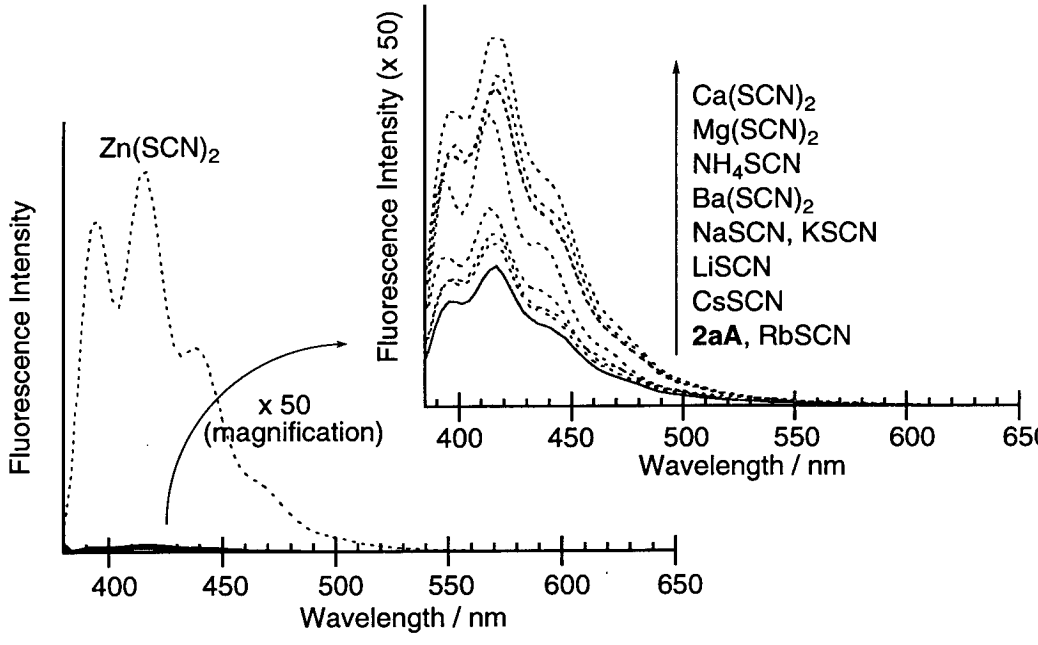

Figure 14. Fluorescence spectra of **2aA** (5.00 x 10^{-6} M) with and without various guest salts (2.5 x 10^{-4} M) in methanol-chloroform (9:1 *v/v*), as excited at 366 nm.

The order depended upon the nature of ionophore properties.[17,18] Interestingly, the fluorescence recovery ($I_{\mathbf{2aA}\text{-Zn complex}}/I_{9\text{-MA}}$=0.93) of **2aA** for Zn^{2+} was larger than that ($I_{\mathbf{2aN}\text{-Zn complex}}/I_{1\text{-MN}}$=0.73)[10] of the corresponding naphthyl derivative (**2aN**). The fluorescence intensity of **2aA**-$Zn(SCN)_2$ complex was similar to that of 9-methylanthracene. This means that the 12-crown-4 derivative carrying two anthryl pendants (**2aA**) has a high fluorescence switch-on ability as PET fluoroionophore.

4.6. Pyrene Derivatives (1P, 2P)[6] — Monomer/Excimer Emission Enhancement

Complexation of *N*-(1-pyrenylmethyl)aza-18-crown-6 (**1P**) with Zn^{2+} increased the host fluorescence intensity by a factor of 13. The emission intensity ($I_{\text{H-G complex}}/I_{\mathbf{1P}}$) was decreased in the following order: Zn^{2+} (15) > Mg^{2+} (9.2) > Ca^{2+}, Ba^{2+} (8.5) > NH_4^+ (7.7) > K^+ (5.3) > Li^+ (4.5) > Rb^+ (3.9) > Cs^+ (2.6) > Na^+ (0.6). The selectivity pattern is distinct from those of the corresponding naphthalene and anthracene derivatives (**1N** and **1A**). Compared with **1N** and **1A**, different features are noted that the $I_{\text{H-G complex}}/I_{\mathbf{1P}}$ for Zn^{2+} complexation was larger than that for Ba^{2+}. Interestingly, the fluorescence recovery ($I_{\text{H-G complex}}/I_{\text{standard}}$) of **1P** was higher than those of the corresponding naphthalene and anthracene derivatives (**1N** and **1A**). It is clearly seen from Figure 15 that the emission intensity increased in the

presence of the guest cation, except for Na^+. The observed enhancement indicates the inhibition of exciplex formation by complexation with a guest salt. Futhermore, it is noteworthy that the **1P**-NaSCN complex exhibited a decrease in its monomer emission intensity relative to that of **1P** itself. This suggests that the observed quenching is due to the presence of thiocyanate anion. A similar quenching by the thiocyanate anion was explained based on the photoinduced electron transfer from this anion to the pyrene chromophore.[1,16]

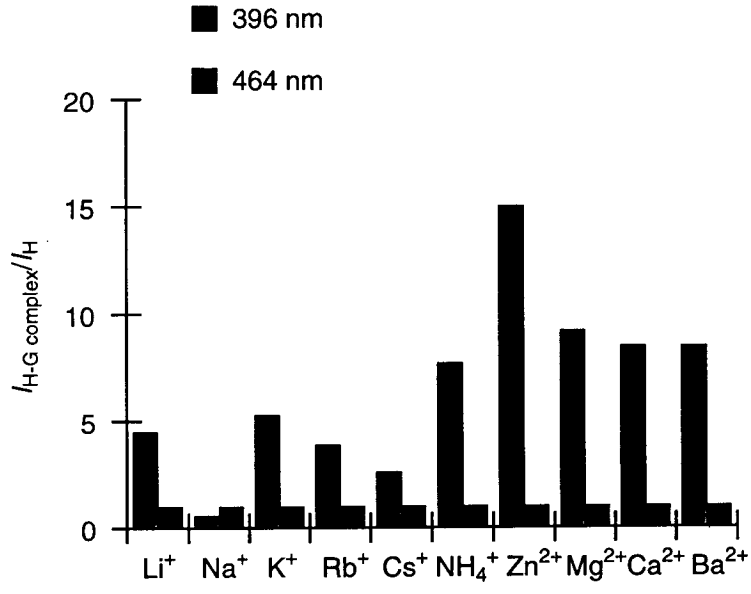

Figure 15. Relative fluorescence intensity changes ($I_{H\text{-}G\ complex}/I_H$) of **1P** ($2.0 \times 10^{-6}$ M) on complex formation with various guest salts (2.0×10^{-2} M).

N,N'-Bis(1-pyrenylmethyl)diaza-18-crown-6 (**2cP**) was found to display unique photophysical properties in the presence of the guest salts. The binding of guest salts to the diazacrown ether (**2cP**) cavity inhibited the exciplex formation and changed the distance between two pyrenyl groups. When the guest salts were added (2×10^4 molar equivalent), the emission-intensitiy ratio changed from 4.4 to 37 at 377–396 nm (monomer emission) and from 1.4 to 14 at 444–474 nm (excimer emission), depending on the nature of the added metal ions, as demonstrated in Figure 16. It is interesting that the ratio (I_{ex} /I_m) of the excimer- (I_{ex}) to monomer- (I_m) emission intensities are different among bound metal ions. The order of this ratio was Na^+ (1.89) > K^+ (0.74) > Rb^+ (0.56) > Cs^+ (0.34) > Li^+ (0.25). This result indicates that the binding of bigger alkali metal ions to the azacrown ether hinders excimer formation to a greater extent. The smaller I_{ex} /I_m values for Li^+ and bivalent metal ions imply that the coordinated structure of these ions differs from that of the other alkali metal ions. From the intensity ratio of the monomer- and excimer- fluorescences of

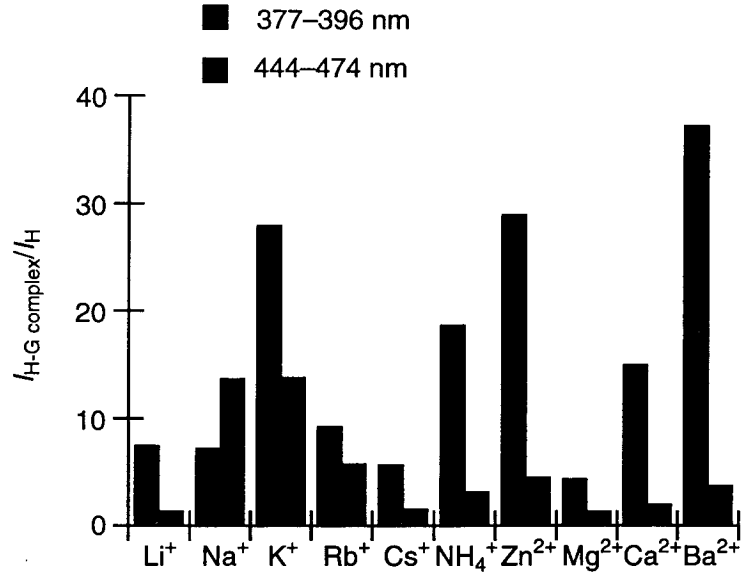

Figure 16. Relative fluorescence intensity changes ($I_{H\text{-}G\ complex}/I_H$) of **2cP** ($1.0 \times 10^{-6}$ M) on complex formation with various guest salts (0.01 – 0.20 M).

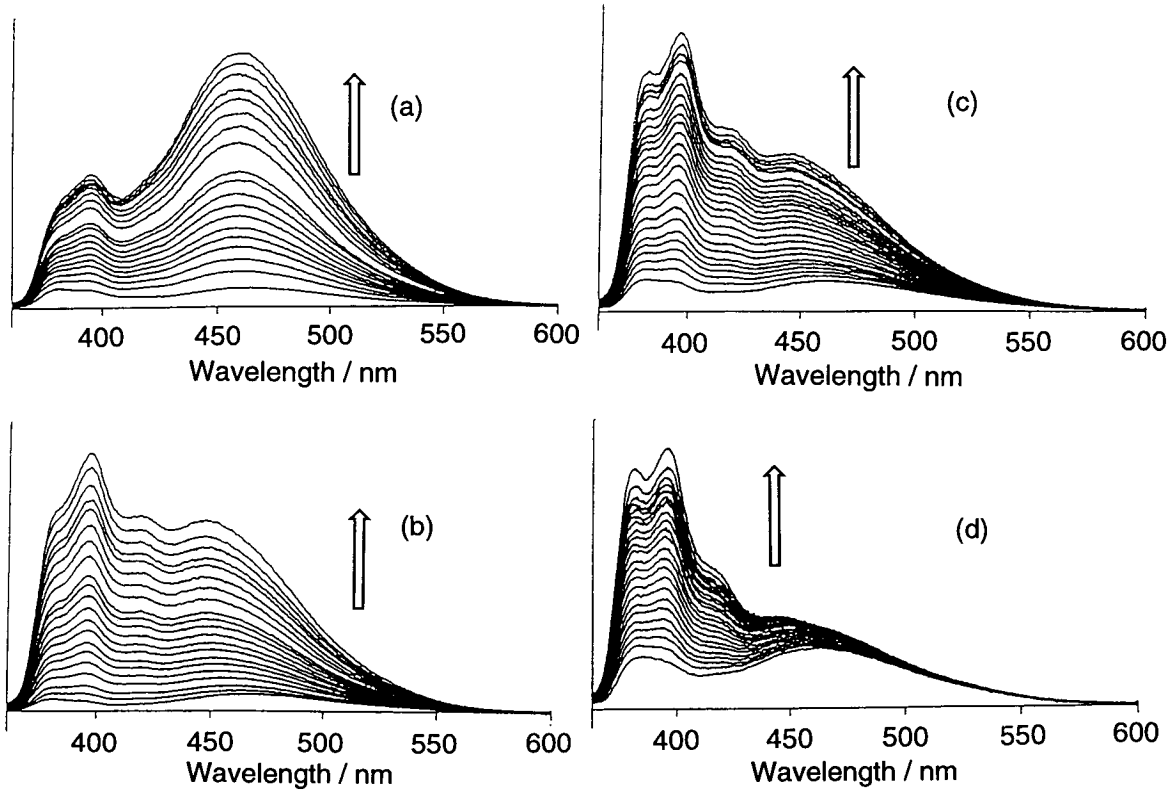

Figure 17. Fluorescence spectra of **2cP** (1.00×10^{-6} M) with and without (a) NaSCN, (b) KSCN, (c) RbSCN, and (d) CsSCN in methanol-chloroform (9:1 *v/v*); [guest salts] = 0 – 0.04 M.

the pyrene pendant, one can estimate the size and the valence of metal ions that were incorporated into the host **2cP**.

NMR Spectral Analysis

Binding interactions of the host (**2cP**) with alkali metal and bivalent metal ions were examined using ^{1}H NMR spectroscopy. When alkali metal salts were added, the resonance peaks shifted downfield or upfield, depending on the nature of the added metal ions (Figure 18c, d).

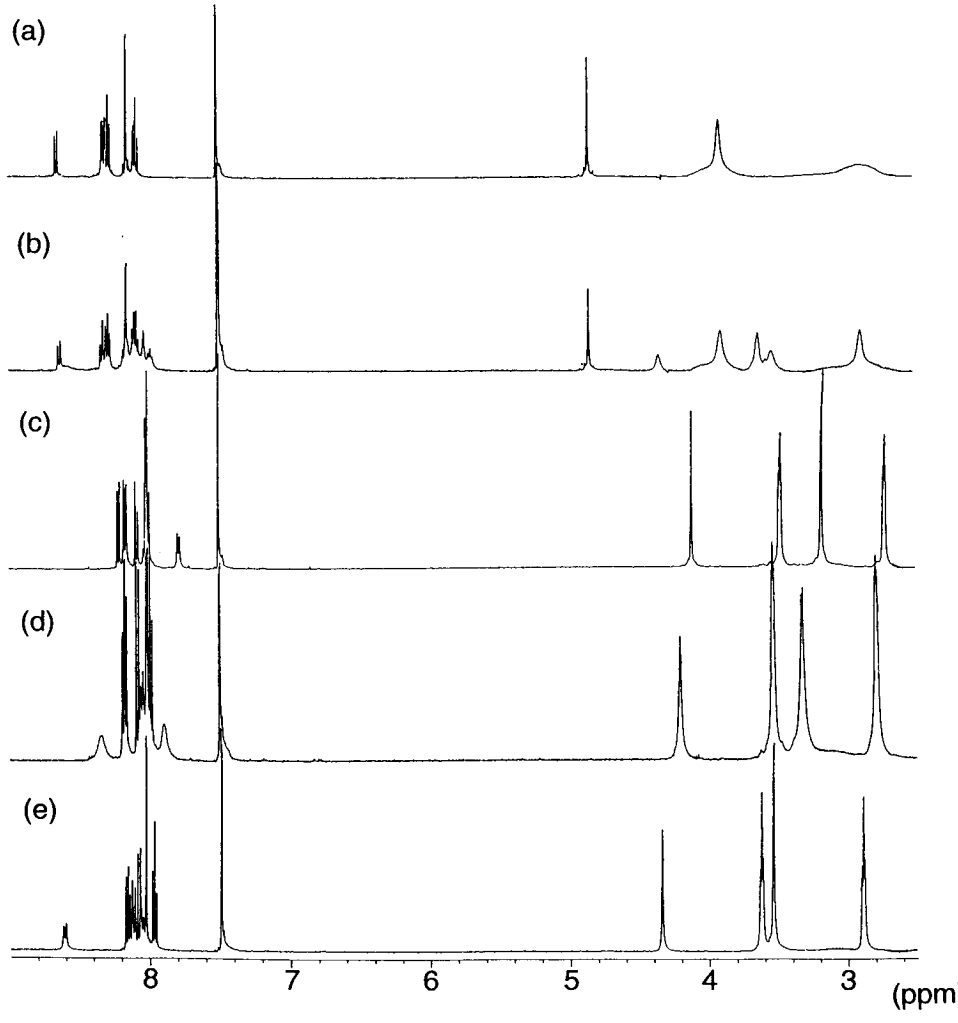

Figure 18. ^{1}H NMR spectral changes of **2cP** (8.0×10^{-4} M) with (a) $Ba(SCN)_2$ (1.4×10^{-3} M), (b) $Ba(SCN)_2$ (2.6×10^{-4} M), (c) KSCN (1.4×10^{-3} M), (d) KSCN (2.6×10^{-4} M), and (e) 0 in CD_3CN-$CDCl_3$ (1:1 *v/v*) at 298 K.

However, the addition of bivalent metal ions decreased the original peak intensities, accompanied by an increase in new resonance-peak intensities (Figure 18a, b). These spectral changes mean that the exchange

rates are different between the alkali-metal and bivalent-metal ions. The gradual upfield shift of the proton signals of the azacrown unit with added KSCN (Figure 18c, d) indicates that the exchange process between a free host and its potassiun complex is rapid compared to the NMR time scale: time-averaged NMR shifts are observed depending upon the guest concentrations. On the other hand, the original (free host, **2cP**) signal intensities decreased, and new resonance-peak intensities (the corresponding complex, [**2cP**-Ba^{2+}]) at 3.90 and 4.84 ppm increased as the $Ba(SCN)_2$ concentration was increased (Figure 18a, b). This finding indicates that the exchange process is slow enough even at room temperature, compared with the NMR time scale, to give new signals corresponding to the barium complex ([**2cP**-Ba^{2+}]). The difference in the exchange rates between K^+ and Ba^{2+} should be responsible for the large difference in the monomer/excimer fluorescence-intensity ratio for there guest cations (Figure 16,17).

Table 5. Changes of ^1H NMR chemical shifts of **2cP** (8.0 x 10^{-4} M) with various guest salts (1.4 x 10^{-3} M)

	Pyrenyl group		Azacrown unit		
	H-10	$-CH_2-$	H_a	H_b	H_c
2cP	8.61	4.35	3.63	3.54	2.89
LiSCN	8.38 (-0.23)	4.32 (-0.03)	3.65 (+0.02)	3.33 (-0.21)	2.82 (-0.07)
NaSCN	8.08 (-0.53)	4.04 (-0.31)	3.36 (-0.27)	3.06 (-0.48)	2.65 (-0.24)
KSCN	8.22 (-0.39)	4.11 (-0.24)	3.47 (-0.06)	3.18 (-0.36)	2.72 (-0.27)
RbSCN	8.34 (-0.27)	4.21 (-0.14)	3.53 (-0.10)	3.28 (-0.26)	2.78 (-0.11)
CsSCN	8.38 (-0.23)	4.23 (-0.12)	3.55 (-0.08)	3.35 (-0.19)	2.80 (-0.09)
$Zn(SCN)_2$	8.46 (-0.15)	4.67 (+0.32)	3.63 (0.00)	3.38 (-0.16)	3.32 (+0.43)
$Mg(SCN)_2$	8.43 (-0.18)	4.67 (+0.32)	3.65 (+0.02)	3.41 (-0.13)	3.09 (+0.20)
$Ca(SCN)_2$	8.85 (+0.24)	5.21 (+0.76)	3.90 (+0.27)	3.90 (+0.36)	3.09 (+0.20)
$Ba(SCN)_2$	8.66 (+0.05)	4.84 (+0.49)	3.90 (+0.27)	3.90 (+0.36)	2.87 (-0.02)

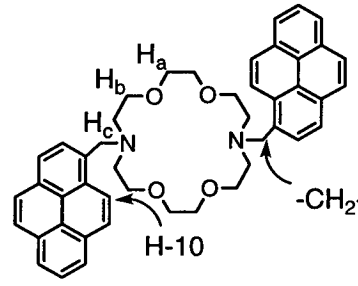

The chemical shifts (δ) and induced shifts (Δδ) of the host (**2cP**) with and without a metal ion are summarized in Table 5. The presence of Ba^{2+} and Ca^{2+} induced a dramatic downfield shift (Δδ=0.49

and 0.76) of the methylene proton signal of the 1-pyrenylmethyl group. There was also a significant downfield shift ($\Delta\delta$=0.36) of the H_b signal of the azacrown unit. This downfield shift is due to an interaction with a metal ion.

On the other hand, Na^+, K^+, Rb^+ and Cs^+ induced distinct upfield shifts of the H signal of the azacrown unit as well as the methylene proton signal of the 1-pyrenylmethyl group. This upfield shift must be due to ring-current effects of the pyrene rings. Interestingly, there were also upfield shifts ($\Delta\delta$= –0.23 — –0.53 ppm) of the H-10 signal of the 1-pyrenyl group, suggesting that an intramolecular interaction between two pyrene rings takes place. As already mentioned, the binding of metal ions to the diazacrown ether caused an emission-intensity enhancement and a large change in the monomer/excimer fluorescence-intensity ratio. The change in the monomer/excimer fluorescence-intensity ratio is considered to result from the metal ion-dependent coordinated structure and exchange rate between the free host (**2cP**) and its guest salt complex in the ground state. In conclusion, the diazacrown ether (**2cP**) having two pyrenyl pendants has a fluorescence sensing properties for the alkali metal(I) ions using the monomer/excimer emission-intensity ratio.

5. Association Constants (*K*)

Guest-salt concentration dependence of the emission intensity allowed us to determine the association constants (*K*) by a nonlinear curve-fitting method[19] (Table 2). The *K* values of the 18-crown-6 derivatives (**1N**, **2cN**, **4bN**, **1A**, **2cA**, **1P**, **2cP**) for K^+ were lower than that[17] of 18-crown-6 (Log *K*=6.32 for $KClO_4$ in MeOH). The order of *K* values for K^+ was **4bN** < **2cN** < **2cA** < **2cP** < **1P** < **1N** < **1A** , indicating that the molecules with two fluorescent pendants substantially inhibit the complexation with guest salts. The *K* values for monoaza-18-crown-6 derivatives (**1N**, **1A**, **1P**) were in reasonable agreement with those available for the parent macrocycles.

While, the selectivity patterns of the diaza-18-crown-6 derivatives (**2cN**, **2cA**, **2cP**) are distinct from those (*K*: $Li^+ < Na^+ < Cs^+ < Rb^+ < K^+ < Ba^{2+}$)[17] of 18-crown-6. The diaza-18-crown-6 derivatives (**2cN**, **2cA**, **2cP**) showed the following guest salt selectivity: (**2cN**: $Li^+ < Ca^{2+} < Cs^+ < Na^+ < Zn^{2+} < Rb^+ < Ba^{2+} < NH_4^+ < K^+ < Mg^{2+}$, **2cA**: $Ca^{2+} < Li^+ < Zn^{2+} < Ba^{2+} < NH_4^+ < Cs^+ < Rb^+ < Na^+ < Mg^{2+} < K^+$, **2cP**: $Li^+ < Zn^{2+} < NH_4^+ < Cs^+ < Ba^{2+} < Ca^{2+} < Rb^+ < Na^+ < Mg^{2+} < K^+$). Compared with 18-crown-6,[17,18] different features are simply noted as follows: (i) a larger *K* value for K^+ complexation than for Ba^{2+} and (ii) a larger *K* value for Na^+ than for Rb^+ and Cs^+. These differences may be explained by the idea that two large fluorophore moieties of **2cN**, **2cA**, **2cP** suppress complexation with larger metal ions (Rb^+ and Cs^+) than Na^+. In spite of the small association constant for **2cP**, the enhancement of the

monomer and/or excimer emission intensity of this host (**2cP**) by bound metal salts establishes that **2cP** has a high fluorescence switch-on ability for complexation within wide concentration range.

Interestingly, the *K* values of 12-crown-4 derivatives (**2aN**, **2aA**) for various guest salts were larger than those of the corresponding 18-crown-6 derivatives (**2cN**, **2cA**). This means that the smaller macrocycle ring may suppress the interaction between two fluorophores and guest salts. The diazacrown derivatives (**2a**, **2c**) showed the following cation selectivity (**2aN**: $NH_4^+ < Cs^+ < Rb^+ < K^+ < Na^+ < Mg^{2+} < Ba^{2+} < Li^+ < Ca^{2+} < Zn^{2+}$, **2cN**: $Li^+ < Ca^{2+} < Cs^+ < Na^+ < Zn^{2+} < Rb^+ < Ba^{2+} < NH_4^+ < K^+ < Mg^{2+}$, **2aA**: $Mg^{2+} < Ba^{2+} < NH_4^+ < Ca^{2+} < Zn^{2+}$, **2cA**: $Ca^{2+} < Li^+ < Zn^{2+} < Ba^{2+} < NH_4^+ < Cs^+ < Rb^+ < Na^+ < Mg^{2+} < K^+$). The diaza-12-crown-4 (**2aA**) exhibited high Zn^{2+} selectivity and fluorescence sensitivity, establishing that **2aA** has a high fluorescence switch-on ability for complexation. The diaza-12-crown-4 having two anthryl pendants may be utilized as a new PET fluorescent sensor for guest salts.

In conclusion, comparison of the selectivity order for **1**–**4** confirms that the size and electronic property of ionophore attached with aromatic pendants may control the selectivity of the host toward guest salts in a delicate manner.

6. X-Ray Crystallographic Analysis

2cN[7] and 2cP[6,20]

The diaza-18-crown-6 derivatives (**2cN**, **2cP**) crystallized nicely. The ORTEP drawings of **2cN** and **2cP** are shown in Figures 19 and 20. The diaza-18-crown-6 derivatives (**2cN**, **2cP**) were centrosymmetric and the two fluorophore units adopt an anti-conformation with the crown-ether ring. The aromatic rings of **2cN** and **2cP** are close to the N atom of the crown ether; the distance between C1 and N1 (2.505 (3) Å) is shorter than the sum of their van der Waals radii [3.05 Å].[21]

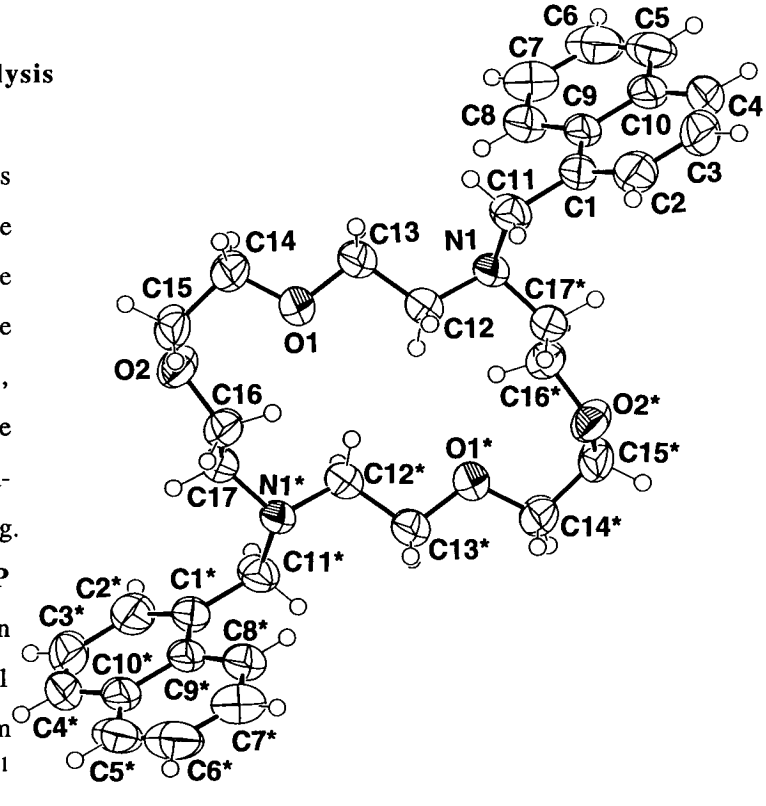

Figure 19. The molecular structure of **2cN** with thermal ellipsoids to enclose 50% probability. Symmetry codes: (*) 1/2 - x, y, 1-z

No π-π interaction is evident in the crystal packing; the distance between

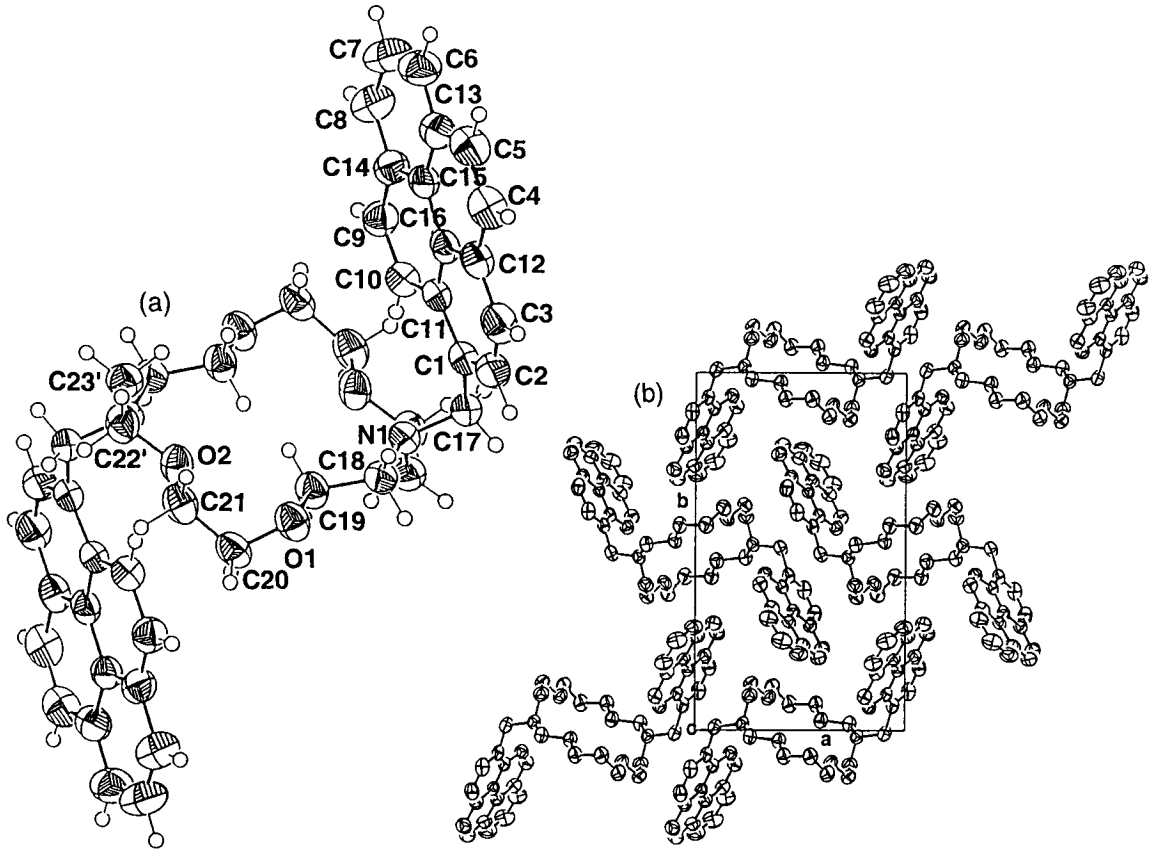

Figure 20. (a) The molecular structure of **2cP** with thermal ellipsoids to enclose 50% probability. Symmetry codes: (*) - x, 1-y, 1-z, (b) Paking diagram of **2cP** view down the *c* axis.

the pyrene planes is greater than 4.0 Å, substantially larger than the width of pyrene itself (3.53 Å), as shown in Figure 20b. The C-N(1) bond lengths (1.464 Å) are not significantly shorter than the single C-N bond length [1.472 (5) Å][21] given by Lide. These mean that intramolecular charge transfer can take place readily between the fluorophore unit and the nitrogen atom in the ground state as well as in the excited singlet state.

2cN-KNCS and 2cN-Ba(NCS)$_2$[22]

Fortunately, the single crystals of **2cN**-KNCS and **2cN**-Ba(NCS)$_2$-H_2O were obtained from mixtures with 1:1 stoichiometry of a methanol solution of metal thiocyante and a $CHCl_3$ solution of **2cN**. The molecular structure of **2cN**-KNCS is shown in Figure 21. The complex has the stoichiometry as **2cN**-KNCS. An ORTEP diagram show that the two naphthalene rings adopt an *anti* conformation with respect to one another across the crown ether ring. The two naphthalene groups are far from each other and do not

interact with the K^+ directly. The K^+ ion sits roughtly at the centre of the hexagon of ligating donor atoms. The six ligating donor atoms are alternately 0.06–0.63 Å above and below their mean plane. The four oxygen and two nitrogen atoms are endodentate. The K^+ ion is surrounded by six donor atoms and thiocyanate anion in a hexagonal pyramidal coordination. The thiocyanate anion sits on K(01) and is displaced 5° from perpendicular position to the crown ring mean plane. The four K(01)–O are K(01)–N distances and not equal (K(01)–O: 2.684—2.837 Å (average 2.74 Å), K(01)–N 3.074 and 3.115 Å (average 3.09 Å)) (that is, the hexagon is slightly deformed). The K(01)–N(16) and K(01)–O(1) distances are longer than those of the other distances. This means that the interaction between two donor atoms (O(1) and N(16)) and K^+ is weak, establishing that the emission intensity of **2cN**-KNCS is lower than that of **2cN**-$Ba(NCS)_2$.

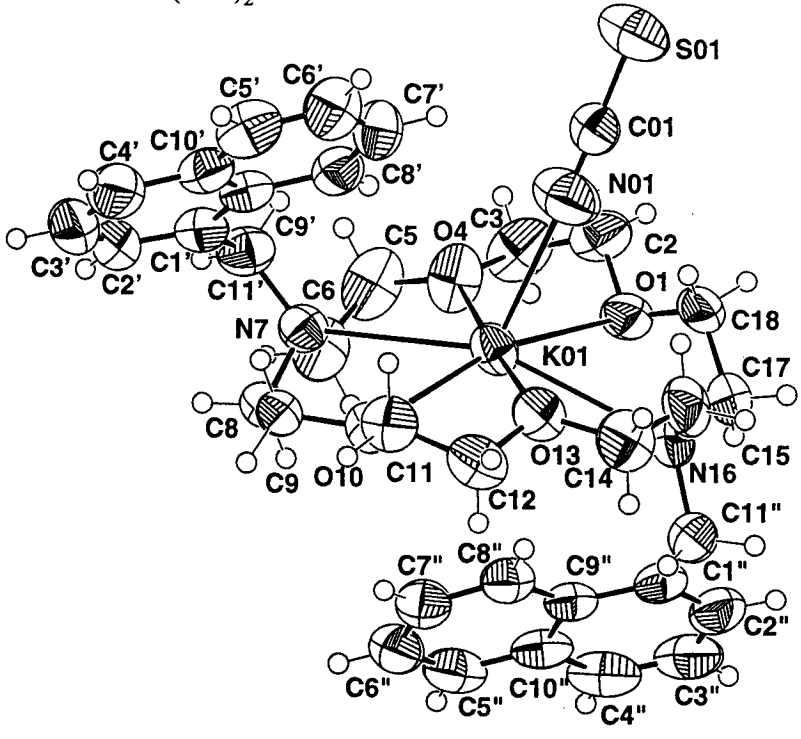

K(01)–O(1)	2.837 (3) Å
K(01)–O(4)	2.684 (3) Å
K(01)–N(7)	3.074 (3) Å
K(01)–O(10)	2.749 (3) Å
K(01)–O(13)	2.695 (3) Å
K(01)–N(16)	3.115 (3) Å

Figure 21. The molecular structure of **2cN**·KNCS with thermal ellipsoids to enclose 50% probability.

The structure of the **2cN**-$Ba(NCS)_2$-H_2O complex differs significantly from that of the **2cN**-KNCS complex. The two naphthalene rings of **2cN**-$Ba(NCS)_2$-H_2O adopt a *syn* conformation with respect to each other as shown in Figure 22. The Ba^{2+} ion is coordinated by the six donor atoms (four oxgen and two nitrogen atoms) of the diazacrown ether, the two nitrogen atoms of the thiocyanate anions on one side (near naphthalene ring) and the oxygen atom of water molecule on the opposite side. The Ba^{2+} ion is displaced 0.17 Å from the mean plane of the diazacrown. In conclusion, the coordinated structure also is

responsible for a large difference in the relative emission-intensity enhancement that was observed in the presence of guest cation.

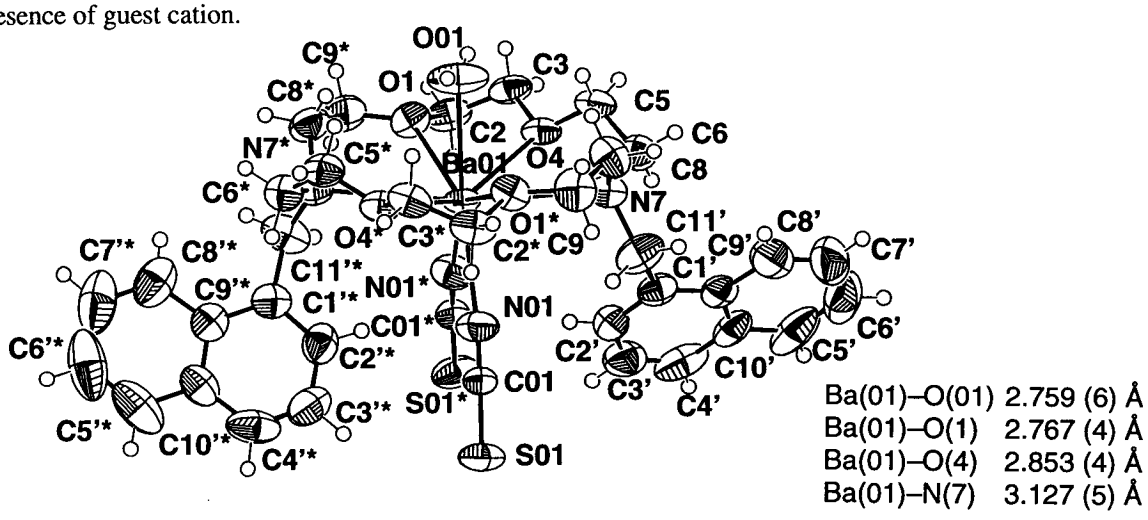

Figure 22. The molecular structure of **2cN**·$Ba(NCS)_2$·H_2O with thermal ellipsoids to enclose 50% probability. Symmetry codes: (*) 1/2 - x, y, 1-z

7. Conclusion

The diazacorwn derivatives carrying two fluorescent pendants (**2**) showed fluorescent enhancement with various guest salts. The diazacrown derivatives have the following properties: 1) the fluorescence quenching of the host itself occurs by intramoleculer electron transfer between the two fluorescent pendants and the two nitrogen atoms in the crown ring, and the cation binding to the host azacrown results in an emision-intensity enhancement; 2) The guest cation-induced emision-intensity enhancement originated from the affinity of the nitrogen atom in the azacrown ether for cations, the guest cation-dependent coordinated structure, and exchange rate between the free host and its guest salt complex in the ground state. Especially, the anthracene-functionalized diaza-12-crown-4 derivative (**2aA**) exhibited Zn^{2+} selectivity and in the presence of this cation the host fluorescence intensity was increased by a factor of 182. The diaza-12-crown-4 derivative (**2aA**) exhibited the higher selectivity and fluorescence sensitivity for Zn^{2+} than the other azamacrocycles, establishing that **2aA** has a high fluorescence switch-on ability for complexation. The diaza-12-crown-4 having two anthryl pendant may be utilized as a new PET fluorescent sensor for guest cations.

While, the binding of metal ions to *N*,*N'*-bis(1-pyrenylmethyl)diaza-18-crown-6 (**2cP**) cavity inhibited the exciplex formation and changed the distance between two pyrenyl groups. This caused not only an emission-intensity enhancement, but also a large change in the monomer/excimer fluorescence-intensity ratio. The change in the monomer/excimer fluorescence-intensity ratio is considered to result from the

metal ion-dependent coordinated structure and exchange rate between the free host (**2cP**) and its metal salt complex in the ground state. The diaza-18-crown-6 (**2cP**) has a fluorescence sensing ability for the alkali metal(I) ions using the monomer/excimer emission-intensity ratio. The diazacrown ether, having two 1-pyrenyl pendants, may be utilized as a new fluorescent sensor for alkali metal ions.

ACKNOULEDGEMENT

We are greateful to Prof. Nobuo Kato and Prof. Akira Mori of Advanced Material Study, Kyushu University for the measurement of X-Ray crystallography. This work was partly supported by a Grant-in-Aid for Encouragement of Young Scientists (No. 10740330) from the Ministry of Education Science, Sports and Culture, Japan.

REFERENCES AND NOTES

1. H. G. Löhr and F. Vögtle, *Acc. Chem. Res.*, 1985, **18**, 65; J. -M. Lehn, *Angew. Chem., Int. Ed. Engl.*, 1988, **27**, 89; D. J. Cram, *ibid.*, 1988, **27**, 1009; J. M. Lehn, "*Supramolecular Chemistry*", VCH Verlagsgesellschaft mbH., Weinheim, 1995.
2. A. W. Czarnik, *Acc. Chem. Res.*, 1994, **27**, 302; L. Fabrizzi and A. Poggi, *Chem. Soc. Rev.*, **1995**, 197; E. Kimura and T. Koike, *Chem. Soc. Rev.*, 1998, **27**, 179.
3. A. P. de Silva and S. A. de Silva, *J. Chem. Soc., Chem. Commun.*, **1986**, 1709.
4. R. A. Bissell, A. P. Silva, H. Q. N. Gunaratne, P. L. M. Lynch, G. E. M. Maguire, and K. R. A. S. Sandanayake, *Chem. Soc. Rev.*, **1992**, 187; A. P. de Silva, H. Q. N. Gunaratne, T. Gunnlaugsson, C. P. McCoy, R. S. Maxwell, J. T. Rademacher and T. E. Rice, *Pure & Appl. Chem.*, 1996, **48**, 1443; A. P. de Silva, H. Q. N. Gunaratne, T. Gunnlaugsson, A. J. M. Huxley, C. P. McCoy, J. T. Rademacher, and T. E. Rice, *Chem. Rev.*, 1997, **97**, 1515.
5. M. Takagi, H. Nakamura, and K. Ueno, *Anal. Lett.*, 1977, **10**, 1115; H. Nishida, Y. Katayama, H. Katsuki, M. Takagi, H. Nakamura, and K. Ueno, *Chem. Lett.*, **1982**, 1853; T. Iyoda, M. Morimoto, N. Kawasaki, and T. Shimidzu, *J. Chem. Soc., Chem. Commun.*, **1991**, 1480; I. Aoki, H. Kawabata, K. Nakashima, and S. Shinkai, *ibid.*, **1991**, 1771; I. Aoki, T. Harada, T. Sakaki, Y. Kawahara, and S. Shinkai, *ibid.*, **1992**, 1341; S. Alihodzic, M. Zinic, B. Klaic, R. Kiralj, B. Kojic-Prodic, M. Herceg, and Z. Cimerman, *Tetrahedron Lett.*, 1993, **34**, 8345; M. Morimoto, K. Fukui, N. Kawasaki, M. Morimoto, K. Hukui, N. Kawasaki, T. Iyoda, and T. Shimidzu, *ibid.*, 1993, **34**, 95; G. E. Collins and L.-S. Choi, *J. Chem. Soc., Chem. Commun.*, **1997**, 1135; J. H. R. Tucker, H. B. Laurent, P. Marsau, S. W. Riley, and J. -P. Desvergne, *ibid.*, **1997**, 1165; B. König, M. Pelka, H. Zieg, T. Ritter, H. B.-Laurent, R. Bonneau, and J.-P. Desvergne, *J. Am. Chem. Soc.*, 1999, **121**, 1681.
6. K. Kubo and T. Sakurai, *Chem. Lett.*, **1996**, 959; K. Kubo and T. Sakurai, *Rep. Inst. Adv. Mat. Study, Kyushu Univ.*, 1996, **10**, 85; K. Kubo, N. Kato, and T. Sakurai, *Bull. Chem. Soc. Jpn.*, 1997, **70**, 3041.

7. K. Kubo, R. Ishige, N. Kato, E. Yamamoto, and T. Sakurai, *Heterocycles*, 1997, **45**, 2365.
8. K. Kubo, R. Ishige, and T. Sakurai, *Heterocycles*, 1998, **48**, 347; K. Kubo, R. Ishige, and T. Sakurai, *Talanta*, in press.
9. K. Kubo, E. Yamamoto, and T. Sakurai, *Heterocycles*, 1997, **45**, 1457; K. Kubo, E. Yamamoto, and T. Sakurai, *Heterocycles*, 1998, **48**, 1477.
10. K. Kubo, E. Yamamoto, and T. Sakurai, *Heterocycles*, 1998, **48**, 2133; K. Kubo, E. Yamamoto, and T. Sakurai, *Rep. Inst. Adv. Mat. Study, Kyushu Univ.*, 1998, **12**, 137.
11. K. Kubo, S. Sakaguchi, and T. Sakurai, *Rep. Inst. Adv. Mat. Study, Kyushu Univ.*, 1998, **12**, 11; K. Kubo, S. Sakaguchi, and T. Sakurai, *Talanta*, in press.
12. K. Kubo, R. Ishige, J. Kubo, and T. Sakurai, *Talanta*, 1999, **48**, 181.
13. "*Handbook of Photochemistry Second Edition, Revised and Expanded*", ed. by S. L. Murov, I. Carmichael, and G. L. Hug, Marcel Dekker, Inc., New York, 1993.
14. H. Leonhardt and A. Weller, *Ber. Bunsen-Ges. Phys. Chem.*, 1963, **67**, 791; R. S. Davidson and K. R. Trethewey, *J. Chem. Soc., Chem. Commun.*, **1976**, 827; N. Mataga and M. Ottolenghi, "*Photophysical Aspects of Exciplexes Molecular Association*", ed. by R. Foster, Academic Press, London, 1979, **2**, pp. 2–79; X.-J. Luo, G. S. Beddard, and G. Porter, *J. Chem. Soc., Faraday Trans. 1*, 1982, **78**, 3467.
15. N. Kh. Petrov, A. I. Shushin, and E. L. Frankevich, *Chem. Phy. Lett.*, 1981, **82**, 339; N. Kh. Petrov, V. N. Borisenko, M. V. Alfimov, T. Fiebig, and H. Staerk, *J. Phy. Chem.*, 1996, **100**, 6368.
16. S. Iwata and K. Tanaka, *J. Chem. Soc., Chem. Commun.*, **1995**, 1491.
17. R. M. Izatt, K. Pawlak, J. S. Bradshaw, and R. L. Bruening, *Chem. Rev.*, 1991, **91**, 1721; R. M. Izatt, K. Pawlak, and J. S. Bradshaw, *Chem. Rev.*, 1995, **95**, 2529; H. Tsukube, *Coord. Chem. Rev.*, 1996, **48**, 1; H. Tsukube, S. Shinoda, Y. Mizutani, M. Okano, K. Takagi, and K. Hori, *Tetrahedron*, 1997, **53**, 3487.
18. B. Spiess, F. Arnaud-Neu, and M.-J. Schwing-Well, *Helv. Chim. Acta*, 1979, **62**, 1531; F. Arnaud-Neu, M. Sanchez, R. Yahya, M. -J. Schwing-Well, and J. -M. Lehn, *ibid.*, 1985, **68**, 456; "*Aza-Crown Macrocycles*", ed. by J. S. Bradshaw, K. E. Krakowiak, and R. M. Izatt, Wiley, New York, 1995.
19. K. A. Connors "*Binding Constants*", John Wiley & Sons, New York, 1987.
20. K. Kubo, N. Kato, and T. Sakurai, *Acta Cryst.*, 1997, **53C**, 132;
21. R. D. Lide, "*Handbook of Chemistry and Physics, 71st edition*", CRC press, Boston, 1990.
22. K. Kubo, T. Sakurai, N. Kato, and A. Mori, *Heterocycles*, 1999, **51**, 1229.

Received, 30th April, 1999